PHILOSOPHICAL TRANSACTIONS OF THE ROYAL SOCIETY A MATHEMATICAL, PHYSICAL & ENGINEERING SCIENCES

# Thermal Conduction in a Composite Circular Cylinder: A New Technique for Thermal Conductivity Measurements of Lunar Core Samples

K. Horai, J. L. Winkler, S. J. Keihm, M. G. Langseth, J. A. Fountain and E. A. West

*Phil. Trans. R. Soc. Lond. A* 1980 **293**, 571-598
doi: 10.1098/rsta.1980.0004

# THERMAL CONDUCTION IN A COMPOSITE CIRCULAR CYLINDER: A NEW TECHNIQUE FOR THERMAL CONDUCTIVITY MEASUREMENTS OF LUNAR CORE SAMPLES†

BY K. HORAI,‡ J. L. WINKLER JR,§ S. J. KEIHM,‡¶
M. G LANGSETH,‡ J. A. FOUNTAIN‖
AND E. A. WEST‖

‡ *Lamont–Doherty Geological Observatory of Columbia University, Palisades New York* 10964, *U.S.A.*
§ *Lockheed Electronics Corporation, Houston, Texas* 77058, *U.S.A.*
‖ *NASA, G.C. Marshall Space Flight Center, Huntsville, Alabama* 35812, *U.S.A.*

(*Communicated by S. K. Runcorn, F.R.S. – Received* 10 *October* 1978
*– Revised* 20 *February* 1979)

## CONTENTS



† Lamont–Doherty Geological Observatory Contribution no. 2896.
¶ Now at Planetary Science Institute, Science Applications Inc., 283 South Lake Avenue, Pasadena, California 91109, U.S.A.

A new technique has been developed for the measurement of the thermal conductivity of lunar core samples. According to this technique, the core sample is heated radiatively from the outside at a known rate, the temperature is measured at the surface of the core-tube, and the thermal conductivity of the sample is determined by comparing the measured temperature with the theory. The technique conforms with the aims of lunar sample preservation in that the sample remains intact after the measurements. The solution, as obtained in this paper, of a thermal conduction equation for a composite circular cylinder, with zero initial temperature and a constant heat-flux at its outer boundary, provides a theoretical basis for the present technique. Because of their mathematical similarity, the corresponding problems for a composite slab or sphere were also solved and the solutions are presented for possible future application to the thermal conductivity measurements. Testing demonstrated the feasibility of the new technique. The thermal conductivity of a simulant lunar soil sample, as determined by the present technique under vacuum conditions at about 300 K for sample densities of 1.47–1.67 g cm$^{-3}$, is 2.05–2.65 $\times$ 10$^{-3}$ W m$^{-1}$ K$^{-1}$, which compares favourably with that of the same sample, 1.61–2.89 $\times$ 10$^{-3}$ W m$^{-1}$ K$^{-1}$ at sample densities of 1.50–1.75 g cm$^{-3}$, as measured under similar conditions by the standard line heat source technique. We describe in detail the experimental apparatus construction and procedure; in particular, the number of precautions taken to preserve the samples from disturbances and to improve the measurement results. This technique was successfully applied to the thermal conductivity measurement of two Apollo 17 drill-core samples. The results, 1.9–4.9 $\times$ 10$^{-3}$ W m$^{-1}$ K$^{-1}$, which is intermediate between the values of thermal conductivity of the lunar regolith determined *in situ* (0.9–1.3 $\times$ 10$^{-2}$ W m$^{-1}$ K$^{-1}$ and those of lunar soil samples measured in the laboratory under simulated lunar surface conditions (0.8–2.5 $\times$ 10$^{-3}$ W m$^{-1}$ K$^{-1}$) presents an important clue to the understanding of heat transportation mechanisms in the lunar regolith.

## Introduction

The thermal conduction of composite solids has been studied by a number of investigators. Jaeger (1941) solved the problem of a composite circular cylinder, of one material from radius $r = 0$ to $r = a$ and of another from $r = a$ to $r = b$, with zero initial temperature and the outer surface $r = b$ maintained at constant temperature, $V_0$, for time $t > 0$. The same composite circular cylinder subject to zero initial temperature and a constant heat flux, $-F_0$, at $r = b$ for $t > 0$ is treated in the present paper.

The solution of this problem can be applied to the thermal conductivity measurements of lunar core samples. It is now widely recognized that the thermal conductivity of the lunar regolith, as determined *in situ*, is nearly an order of magnitude higher than that of the lunar soil, a major constituent of the lunar regolith, as measured in the laboratory. The thermal conductivity of the lunar regolith, at a depth of 35–235 cm below the lunar surface, as determined from temperature measurements of Apollo 15 and 17 lunar heat flow experiments, is in the range of 0.9–1.3 $\times$ 10$^{-2}$ W m$^{-1}$ K$^{-1}$ (Langseth *et al.* 1976); whereas the thermal conductivity of lunar soil samples returned by Apollo 15, 17 and other missions, as measured in the laboratory under simulated lunar surface conditions, ranges from 0.8 to 2.5 $\times$ 10$^{-3}$ W m$^{-1}$ K$^{-1}$ (Cremers 1972, 1975; Cremers & Birkebak 1971; Cremers & Hsia 1973, 1974; Cremers *et al.* 1970).

The cause of the higher thermal conductivity of the lunar regolith as determined *in situ* has not been clarified. It is known that the thermal conduction in a particulate material, such as the lunar soil, under vacuum conditions is strongly influenced by its intergranular thermal contact. It is conceivable that the state of the thermal contact between the grains of the lunar regolith material, greatly enhanced by a mechanical process characteristic of the lunar surface, such as meteoritic impacts, is the cause of the higher thermal conductivity of the lunar regolith as

measured *in situ*. To test this hypothesis in a laboratory, it is essential that the lunar soil sample used for the measurement maintain its *in situ* intergranular thermal contact configuration as closely as possible. Of the many returned lunar samples, only the drill and drive-tube core samples offer any chance of preserving their original *in situ* heat transport properties because they were recovered by a sampling tube penetrating to a depth of a few metres into the lunar regolith. For this reason, an experimental study of the thermal conductivity of lunar core samples was highly desirable. Severe constraints had to be followed to ensure that no mechanical disruption of the sample occur during the measurements. In addition, excessive thermal and chemical contamination of the samples could not be tolerated since the core samples were to be utilized for many other laboratory investigations.

None of the conventional techniques for thermal conductivity measurements meets these requirements, and a new method had to be developed to suit our purpose. The method chosen was to heat the core sample from the outside at a known rate and measure the rise in temperature at the surface of the core-tube. Because the temperature at the surface, increasing with time, is a function of the thermal properties of both the core-tube and the sample, the thermal properties of the sample can be estimated by comparing the measured temperature with the theory, provided that the thermal properties of the core-tube are known. Thus it is not necessary to extract the sample from the core-tube to make the measurements. Neither is it necessary to insert a heater, or temperature sensor, into the sample within the core-tube, as would be required if another method were applied. The sample remains intact after the measurements. The temperature change in the sample can be kept to a minimum as long as the thermal conductivity determination is possible with a reasonable precision. If the radiative method of heat transfer is chosen, the core-tube will only be in mechanical contact with the sample holder and a sensor attached to the core tube to measure the surface temperature, thereby greatly reducing the possibility of disturbing the sample. It is considered the most favourable technique for thermal conductivity measurements on lunar core samples.

A solution of the thermal conduction equation for a composite circular cylinder is required for the present technique of thermal conductivity measurements. Here we will only indicate the equations to be solved, the boundary and initial conditions to be satisfied and the solutions. Solution derivations by the Laplace transform method will be outlined briefly in appendix A. In deriving the solutions, we found it instructive to solve similar problems for a composite slab and a composite sphere. The composite slab was treated strictly analogously to the composite circular cylinder. The corresponding problem for a composite sphere was solved by changing the variables by a simple transformation. For possible future applications of these problems to the measurements of thermal conductivity, we have given the solutions in appendixes B and C.

## Theory

### *The general case*

We are dealing with heat conduction in the composite circular cylinder of one material for $0 \leqslant r \leqslant a$, and of another for $a \leqslant r \leqslant b$, with zero initial temperature and a constant heat flux $-F_0$ at $r = b$ for time $t > 0$.

Let $v_1$, $k_1$, $\rho_1$, $c_1$ and $\kappa_1 = k_1/\rho_1 c_1$ be the temperature, thermal conductivity, density, specific heat and thermal diffusivity in the inner cylinder $0 \leqslant r \leqslant a$ and $v_2, k_2, \rho_2, c_2$ and $\kappa_2 = k_2/\rho_2 c_2$, the corresponding quantities in the outer cylinder $a \leqslant r \leqslant b$ (figure 1).

The equations to be solved are

$$\frac{\partial^2 v_1}{\partial r^2}+\frac{1}{r}\frac{\partial v_1}{\partial r}-\frac{1}{\kappa_1}\frac{\partial v_1}{\partial t}=0, \quad 0\leqslant r\leqslant a, \quad t>0, \tag{1}$$

$$\frac{\partial^2 v_2}{\partial r^2}+\frac{1}{r}\frac{\partial v_2}{\partial r}-\frac{1}{\kappa_2}\frac{\partial v_2}{\partial t}=0, \quad a\leqslant r\leqslant b, \quad t>0, \tag{2}$$

with the conditions

$$k_2\,\partial v_2/\partial r=-F_0, \quad r=b, \quad t>0, \tag{3}$$

$$v_1=v_2, \quad r=a, \quad t>0, \tag{4}$$

$$k_1\,\partial v_1/\partial r=k_2\,\partial v_2/\partial r, \quad r=a, \quad t>0, \tag{5}$$

$$\partial v_1/\partial r=0, \quad r=0, \quad t>0, \tag{6}$$

and

$$v_1=0\,(0\leqslant r\leqslant a), \quad v_2=0\,(a\leqslant r\leqslant b), \quad t=0. \tag{7}$$

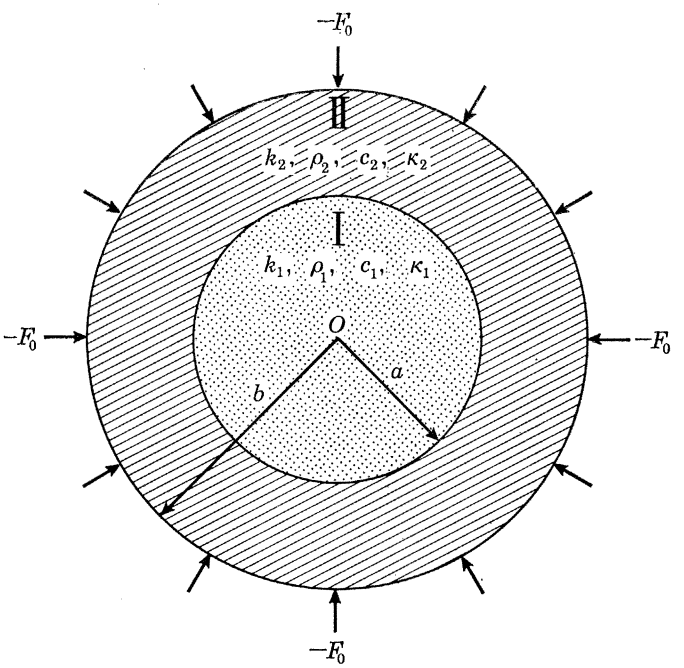


FIGURE 1. Thermal conduction in a composite circular cylinder. Inner cylinder: radius, $a$; thermal conductivity, $k_1$; density, $\rho_1$; specific heat, $c_1$; thermal diffusivity, $\kappa_1$. Outer cylinder: radius, $b$; thermal conductivity, $k_2$; density, $\rho_2$; specific heat, $c_2$; thermal diffusivity, $\kappa_2$. Initial temperature zero. A constant heat flux $-F_0$ at the outer boundary $r=b$ for time $t>0$.

The solutions

$$v_1=-2bF_0\left[\frac{t+r^2/4\kappa_1}{(k_1/\kappa_1)\,a^2+(k_2/\kappa_2)\,(b^2-a^2)}\right.$$
$$\left.-\frac{\dfrac{k_1}{\kappa_1}\left\{\dfrac{a^4}{8\kappa_1}-\dfrac{a^2(b^2-a^2)}{4\kappa_2}+\dfrac{a^2b^2}{2\kappa_2}\ln\dfrac{b}{a}\right\}+\dfrac{k_2}{\kappa_2}\left\{\dfrac{a^2(b^2-a^2)}{4\kappa_1}+\dfrac{b^4-a^4}{8\kappa_2}-\dfrac{a^2b^2}{2\kappa_2}\ln\dfrac{b}{a}\right\}}{\{(k_1/\kappa_1)\,a^2+(k_2/\kappa_2)\,(b^2-a^2)\}^2}\right.$$
$$\left.-\sum_{s=1}^{\infty}\mathrm{e}^{-\kappa_1\alpha_s^2 t}\,J_0(\alpha_s r)\,\Psi(\alpha_s)\right], \tag{8}$$

$$v_2 = -2bF_0\Bigg[\frac{t+\frac{a^2}{4\kappa_1}+\frac{r^2-a^2}{4\kappa_2}+\frac{a^2}{2}\left(\frac{k_1}{k_2}\frac{1}{\kappa_1}-\frac{1}{\kappa_2}\right)\ln\frac{r}{a}}{(k_1/\kappa_1)\,a^2+(k_2/\kappa_2)\,(b^2-a^2)}$$

$$-\frac{\frac{k_1}{\kappa_1}\left\{\frac{a^4}{8\kappa_1}-\frac{a^2(b^2-a^2)}{8\kappa_2}+\frac{a^2b^2}{2\kappa_2}\ln\frac{b}{a}\right\}+\frac{k_2}{\kappa_2}\left\{\frac{a^2(b^2-a^2)}{4\kappa_1}+\frac{b^4-a^4}{8\kappa_2}-\frac{a^2b^2}{2\kappa_2}\ln\frac{b}{a}\right\}}{\{(k_1/\kappa_1)\,a^2+(k_2/\kappa_2)\,(b^2-a^2)\}^2}$$

$$+\sum_{s=1}^{\infty}\mathrm{e}^{-\kappa_1\alpha_s^2 t}\,\tfrac{1}{2}\pi\kappa a\alpha_s\left[J_0(a\alpha_s)\left\{J_0(r\kappa\alpha_s)\,Y_1(a\kappa\alpha_s)-Y_0(r\kappa\alpha_s)\,J_1(a\kappa\alpha_s)\right\}\right.$$

$$\left.-(k_1/\kappa k_2)\,J_1(a\alpha_s)\left\{J_0(r\kappa\alpha_s)\,Y_0(a\kappa\alpha_s)-Y_0(r\kappa\alpha_s)\,J_0(a\kappa\alpha_s)\right\}\right]\Psi(\alpha_s)\Bigg], \tag{9}$$

where

$$\kappa \equiv \sqrt{(\kappa_1/\kappa_2)}, \tag{10}$$

$$\begin{aligned}\Psi(\alpha_s)^{-1} \equiv\ & \tfrac{1}{2}\pi ab\kappa\kappa_1\alpha_s^3\left[(k_1/\kappa_1)\,\kappa b\,J_1(a\alpha_s)\left\{J_0(b\kappa\alpha_s)\,Y_0(a\kappa\alpha_s)-Y_0(b\kappa\alpha_s)\,J_0(a\kappa\alpha_s)\right\}\right.\\ &-(k_2/\kappa_2)\,b\,J_0(a\alpha_s)\left\{J_0(b\kappa\alpha_s)\,Y_1(a\kappa\alpha_s)-Y_0(b\kappa\alpha_s)\,J_1(a\kappa\alpha_s)\right\}\\ &+\{(k_2-k_1)/\kappa_1\}\,\kappa a\,J_1(a\alpha_s)\left\{J_1(b\kappa\alpha_s)\,Y_1(a\kappa\alpha_s)-Y_1(b\kappa\alpha_s)\,J_1(a\kappa\alpha_s)\right\}\\ &\left.-(k_2/\kappa_2-k_1/\kappa_1)\,a\,J_0(a\alpha_s)\left\{J_1(b\kappa\alpha_s)\,Y_0(a\kappa\alpha_s)-Y_1(b\kappa\alpha_s)\,J_0(a\kappa\alpha_s)\right\}\right]\end{aligned} \tag{11}$$

and $\alpha_s$, $s = 1, 2, \ldots$ are the positive roots of

$$\begin{aligned}&J_0(a\alpha)\left\{J_1(b\kappa\alpha)\,Y_1(a\kappa\alpha)-Y_1(b\kappa\alpha)\,J_1(a\kappa\alpha)\right\}\\ &\qquad=(k_1/\kappa k_2)\,J_1(a\alpha)\left\{J_1(b\kappa\alpha)\,Y_0(a\kappa\alpha)-Y_1(b\kappa\alpha)\,J_0(a\kappa\alpha)\right\}\end{aligned} \tag{12}$$

for $\alpha$.

In the above, $J_n(x)$ and $Y_n(x)$ with $n = 0$ and 1 are the Bessel functions of the first kind and the second kind with the real variable $x$ in conformity with the usage as given by Watson (1966).

*The same problem as above – a special case of $k_2 = \infty$*

The lunar core samples are contained in metal tubes. For example, the Apollo 15 type drill core samples are contained in a tube of titanium alloy, Ti–6Al–4V with a thermal conductivity of 7.4 $\mathrm{W\,m^{-1}\,K^{-1}}$ at 300 K, or a thousand times more conductive than the lunar regolith material at the same temperature. Therefore, if the wall of the tube is thin and the rate of heating not excessive, resulting in a small temperature difference across the wall, the assumption that $k_2 = \infty$ is justified and the solution obtained below can be used in experimental data analyses.

The solution to this problem is derived by taking a limit of $k_2 \to \infty$ in the foregoing formulas. However, it is equally easily obtained by solving the following corresponding equation

$$\frac{\partial^2 v_1}{\partial r^2}+\frac{1}{r}\frac{\partial v_1}{\partial r}-\frac{1}{\kappa_1}\frac{\partial v_1}{\partial t}=0, \quad 0 \leqslant r \leqslant a, \quad t>0, \tag{13}$$

with the conditions

$$2\pi a k_1\frac{\partial v_1}{\partial r}+\pi(b^2-a^2)\,c_2\rho_2\frac{\partial v_1}{\partial t}=-2\pi bF_0, \quad r=a, \quad t>0, \tag{14}$$

$$\partial v_1/\partial r = 0, \quad r=0, \quad t>0, \tag{15}$$

and

$$v_1 = 0\,(0 \leqslant r \leqslant a), \quad t=0. \tag{16}$$

The second term on the left hand side of equation (14) represents the isothermal heating of the outer cylinder.

The solution is

$$v_1 = -2bF_0\left(\frac{t+(r^2-a^2)/4\kappa_1}{(b^2-a^2)\,c_2\rho_2+a^2c_1\rho_1}+\frac{(a^4/8\kappa_1)\,c_1\rho_1}{\{(b^2-a^2)\,c_2\rho_2+a^2c_1\rho_1\}^2}\right.$$
$$\left.-\sum_{s=1}^{\infty}\mathrm{e}^{-\kappa_1\alpha_s^2 t}\{J_0(r\alpha_s)/J_0(a\alpha_s)\}\,\Psi(\alpha_s)\right), \tag{17}$$

where
$$\Psi(\alpha_s)^{-1}\equiv\kappa_1\alpha_s^2\left(\tfrac{1}{4}(b^2-a^2)\frac{(c_2\rho_2)^2\alpha_s^2}{c_1\rho_1}+(b^2-a^2)\,c_2\rho_2+a^2c_1\rho_1\right) \tag{18}$$

and $\alpha_s (s = 1, 2, \ldots)$ are the positive roots of

$$\frac{\frac{1}{2}(b^2-a^2)\,c_2\rho_2}{a^2c_1\rho_1}a\alpha J_0(a\alpha)+J_1(a\alpha)=0 \tag{19}$$

for $\alpha$. For the temperature in $a \leqslant r \leqslant b$, we obtain from equation (17)

$$v_2\equiv v_1|_{r=a}$$
$$=-2bF_0\left(\frac{t}{(b^2-a^2)\,c_2\rho_2+a^2c_1\rho_1}+\frac{(a^4/8\kappa_1)c_1\rho_1}{\{(b^2-a^2)\,c_2\rho_2+a^2c_1\rho_1\}^2}-\sum_{s=1}^{\infty}\mathrm{e}^{-\kappa_1\alpha_s^2 t}\,\Psi(\alpha_s)\right), \tag{20}$$

which is constant as a function of $r$ in $a \leqslant r \leqslant b$.

### *The properties of the solution*

We wish to study in detail the properties of solution (20) because it will be used in experimental data analyses. Firstly, to compute $v_2$ as a function of time $t$, it is necessary to evaluate the $\alpha_s$s from equation (19). Since $\frac{1}{2}(b^2-a^2)\,c_2\rho_2/a^2c_1\rho_1 > 0$, equation (19) can have a root only in an interval in which $J_0(x)$ and $J_1(x)$ have opposite signs. As an elementary theory of Bessel function shows, the signs of $J_0(x)$ and $J_1(x)$ are opposite in the intervals $j_{0,n} < x < j_{1,n}$ where $j_{0,n}$ and $j_{1,n}$ are the $n$th positive roots of $J_0(x)$ and $J_1(x)$. In all of these intervals, $J_1(x)/J_0(x)$ is a monotonically increasing function ranging from $-\infty$ to 0. Hence equation (19) has a single solution in each of these intervals

$$j_{0,n} < a\alpha_n < j_{1,n}, \quad n = 1, 2 \ldots . \tag{21}$$

Since $j_{0,n}$s and $j_{1,n}$s are known (see, for example, Watson (1966) in which the values of $j_{0,n}$s and $j_{1,n}$s are tabulated from $n = 1$ to 40), the computation of $\alpha_n$s are greatly facilitated by the use of relation (21).

The computation of $v_2$ by equation (20) involves the evaluation of the series that must be terminated after a certain number of terms so that the remainder becomes negligibly small compared with the partial sum. The degree of convergence can be estimated in the following way. Since $v_2 = 0$ for $t = 0$, by putting $t = 0$ in equation (20) we obtain the relation

$$S\equiv\frac{(a^4/8\kappa_1)\,c_1\rho_1}{\{(b^2-a^2)\,c_2\rho_2+a^2c_1\rho_1\}^2}=\sum_{s=1}^{\infty}\Psi(\alpha_s), \tag{22}$$

by use of which we can choose the number of terms $N$ that makes

$$\sum_{s=N+1}^{\infty}\Psi(\alpha_s)\Big/\sum_{s=1}^{\infty}\Psi(\alpha_s)=\left\{S-\sum_{s=1}^{N}\Psi(\alpha_s)\right\}\Big/S<\epsilon, \tag{23}$$

where $\epsilon < 1$ is a desired criterion. If we note that, for $t > 0$,

$$1 > \mathrm{e}^{-\kappa_1\alpha_s^2 t} \quad \text{and} \quad \mathrm{e}^{-\kappa_1\alpha_s^2 t} > \mathrm{e}^{-\kappa_1\alpha_{s+1}^2 t} \quad (s = 1, 2, \ldots), \tag{24}$$

it can be shown easily that, for the value of $N$ as chosen above, a relation

$$\left\{\sum_{s=N+1}^{\infty} e^{-\kappa_1 \alpha_s^2 t}\, \Psi(\alpha_s)\right\} \Big/ \left\{\sum_{s=1}^{\infty} e^{-\kappa_1 \alpha_s^2 t}\, \Psi(\alpha_s)\right\} < \epsilon \tag{25}$$

also holds.

So far, we have discussed the solutions obtained when the heat flux across the boundary is constant as a function of time. In order to deal with the experimental data, it is desirable to provide a solution in which the heat flux across the boundary varies with time. A rigorous solution when the heat flux across the boundary is an arbitrary function of time, $-F(\tau)$, is beyond the scope of this paper. Instead, we will seek an approximate solution useful in data analyses.

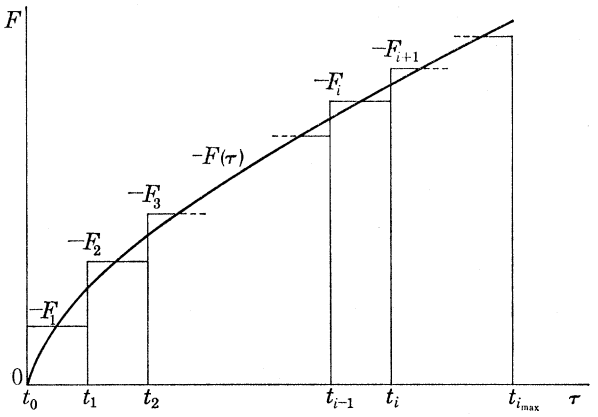


FIGURE 2. Continuous and slowly varying heat input, $-F(\tau)$, as a function of time $\tau$, approximated by a stepwise varying function, $-F_i$, $(t_{i-1} \leqslant \tau \leqslant t_i)$, $i = 1, 2 \ldots, i_{\max}$.

If $-F(\tau)$ is a slowly varying function of time $\tau$, it can be approximated by a stepwise varying function

$$-F_i \equiv \frac{1}{t_i - t_{i-1}} \int_{t_{i-1}}^{t_i} \{-F(\tau)\}\, d\tau, \quad (i = 1, 2, \ldots, i_{\max}), \tag{26}$$

that is constant in the interval between $t_{i-1}$ and $t_i$ (figure 2). By writing the solution given in equation (20) by $v_2(t, -F_0)$ to denote the heating effect of a constant heat flux, $-F_0$, after time $t$, the effect of heating due to the solitary heat flux

$$-F(\tau) = \begin{cases} 0 & (0 \leqslant \tau < t_{i-1}), \\ -F_i & (t_{i-1} \leqslant \tau < t_i), \\ 0 & (t_i \leqslant \tau < t), \end{cases}$$

is given by $v_2(t - t_{i-1}, -F_i) - v_2(t - t_i, -F_i)$ by virtue of the principle of superposition of solutions for the linear differential equation. According to the same principle, the solution for the stepwise varying heat flux $-F(\tau) = -F_i$, $(t_{i-1} \leqslant \tau < t_i)$, $i = 1, 2, \ldots, i_{\max}$ is obtained as

$$\begin{aligned} v_2 &= \sum_{i=1}^{i_{\max}} \{v_2(t - t_{i-1}, -F_i) - v_2(t - t_i, -F_i)\} \\ &= -2b \sum_{i=1}^{i_{\max}} F_i \left[ \frac{t_i - t_{i-1}}{(b^2 - a^2)\, c_2 \rho_2 + a^2 c_1 \rho_1} - \sum_{s=1}^{\infty} e^{-\kappa_1 \alpha_s^2 t} \left(e^{\kappa_1 \alpha_s^2 t_{i-1}} - e^{\kappa_1 \alpha_s^2 t_i}\right) \Psi(\alpha_s) \right], \end{aligned} \tag{27}$$

where $t = t_{i_{\max}}$.

## Experimental method

The theory developed in the preceding section was applied to thermal conductivity measurements of lunar core samples. Experiments were conducted to put the theory into practice with two objectives: (1) to demonstrate the feasibility of the present measurment technique, and (2) to insure that the measuring apparatus complied with N.A.S.A.'s criteria for the handling of lunar samples returned by Apollo missions. We will now describe briefly the methods and results of these test measurements.

### *Apparatus*

Figure 3 illustrates the experimental arrangement for the measurements of Apollo 15 type drill core samples. The sample's core-tube is 42.54 cm long, 2.04 cm in inner diameter and 2.33 cm outer diameter. The heater is a hollow circular cylinder, concentric to the core-tube, 30.23 cm long with inner and outer diameters of 3.56 cm and 4.92 cm respectively. The heater position is adjustable to enable a determination of the thermal conductivity to be made at several locations along the length of the core tube. Adjustment of the heater position is made by the use of a screw rod connected to the mechanical feedthrough attached to the flange of the vacuum chamber. The heater temperature is raised by passing an electric d.c. current through the heating wire wound on the core of the heater. For temperature measurements, copper–constantan thermocouples attached to the surfaces of the heater and core tube are used.

The choice of materials constituting the experimental apparatus is restricted. To avoid a possible chemical contamination of the lunar material, the apparatus parts, as shown in figure 3, having a possible direct contact with the lunar sample, are made of materials such as aluminium, stainless steel and Teflon, admissible by N.A.S.A. standards. The use of a copper–constantan thermocouple is admitted provided that the wire be Teflon coated, except close to a junction.

An accurate temperature measurement at the heater and core-tube surfaces is essential to determine the thermal conductivity by the present technique. For purposes of lunar sample preservation, the use of an organic heat sink compound as a means of improving the thermal contact is prohibited. For core-tube surface temperature measurements, use is made of a copper circular disk, 1.2 mm thick and 4 mm in diameter, with a hole drilled from the side surface of the disk to the centre where the junction of no. 30 thermocouple wires has been inserted. The disk is pressed against the axial direction so that the thermocouple junction is held tightly by the collapsed hole. The tool has been so designed that, by pressing it, one of the disk's flat surfaces acquires the same curvature as that of the core-tube's round surface. The disk is attached to the core-tube by a polyimide band, 6 mm wide and 55 mm long, placed on the disk and encircling the core-tube circumference with its ends tied by stainless steel spiral springs to ensure contact between disk and core-tube by tension of the springs.

A similar device is used to measure the temperature at the heater's surface. A rectangular parallelepiped piece of copper, 1.2 mm × 3.5 mm × 9 mm, with a hole containing the thermocouple junction drilled on one of the two end surfaces, is embedded into a groove, 1.2 mm deep and 3.5 mm wide, cut on the inner surface of the heater along its length, and tightened to the heater by a stainless steel screw. As the thermocouple junction is thus connected to the heater by thermally conductive metals, the junction remains isothermal to the heater's inner surface.

*Heat transfer from the heater to the core-tube*

A formula for the radiative heat transfer from the heater to the core-tube, as a function of heater and core-tube surface temperatures, has been described in theory (see, for example, Gröber *et al.* 1961). For a system of infinitely long concentric circular cylinders, the radiative heat exchange between the inner cylinder (radius $r_1$, surface temperature $T_1$ and surface thermal

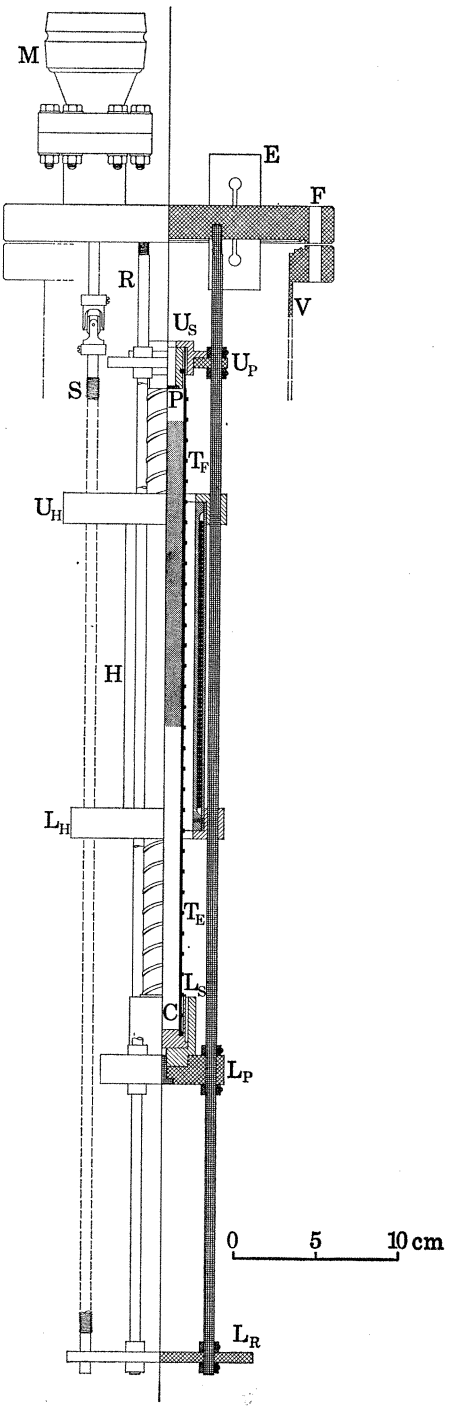


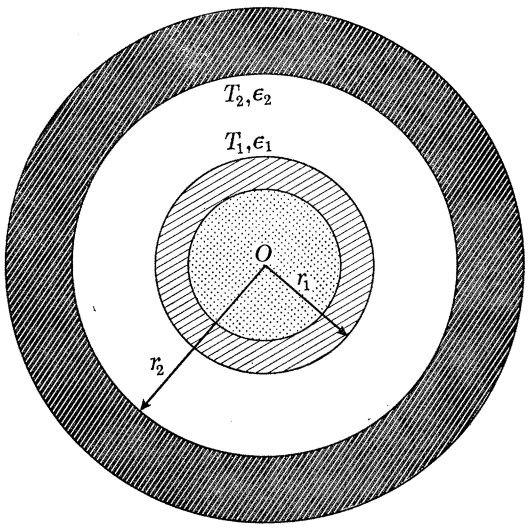


FIGURE 4. Radiative thermal exchange between concentric circular cylinders of infinite axial extent. Radius of inner cylinder, $r_1$; surface temperature, $T_1$; surface thermal emissivity, $\epsilon_1$. Inner radius of outer cylinder, $r_2$; surface temperature, $T_2$; surface thermal emissivity, $\epsilon_2$.

FIGURE 3. Experimental arrangement for the Apollo 15 type drill core sample thermal conductivity measurement. Left half: outside view. Right half: section through the core-tube axis. $T_F$, core-tube, filled with the sample; $T_E$, empty core-tube; C, core-tube cap (Teflon); P, core-tube plug (Teflon); H, heater, core (anodized aluminium 6061-T6), jacket (aluminium 6061-T6), heating wire (Teflon coated constantan); $U_H$, upper heater holder (Teflon); $L_H$, lower heater holder (Teflon); S, screw rod, or driving shaft (stainless steel 300 SST); R, supporting rods (stainless steel 300 SST); $U_P$, upper sample holder plate (anodized aluminium 6061-T6); $U_S$, upper sample holder (Teflon); $L_P$, lower sample holder plate (anodized aluminium 6061-T6); $L_S$, lower sample holder (Teflon); $L_R$, lower supporting ring (anodized aluminium 6061-T6); M, direct drive motion (mechanical) feedthrough; E, electrical feedthrough; V, vacuum chamber (stainless steel 300 SST); F, vacuum chamber flange (stainless steel 300 SST). The thermocouple wires are not shown.

emissivity $\epsilon_1$) and the outer cylinder (radius $r_2$, surface temperature $T_2$ and surface thermal emissivity $\epsilon_2$) per unit time, per unit length of the cylindrical system is given by

$$Q = \frac{A_1 \sigma_b (T_2^4 - T_1^4)}{1/\epsilon_1 + (A_1/A_2)(1/\epsilon_2 - 1)}, \tag{28}$$

where $\sigma_b$ is the Stefan–Boltzman constant; $A_1 = 2\pi r_1$ and $A_2 = 2\pi r_2$ are the surface areas, per unit length, of the inner and outer cylinders (figure 4).

In measuring the thermal conductivity of lunar core samples, it is desirable to keep the variation in sample temperatures as small as possible. Equation (28) can be simplified for small temperature variations. If $T_0$ is the initial equilibrium temperature and the variations in the heater and core tube surface temperatures are $T_2 = T_0 + \delta T_2$ and $T_1 = T_0 + \delta T_1$ where $\delta T_1 \ll T_0$ and $\delta T_2 \ll T_0$ respectively, then equation (28) can be approximated

$$Q = \frac{4A_1 \sigma_b T_0^3}{1/\epsilon_1 + (A_1/A_2)(1/\epsilon_2 - 1)} (\delta T_2 - \delta T_1). \tag{29}$$

In this expression, the rate of heat transfer by radiation from the heater to the core-tube is proportional to the difference in surface temperatures between the heater and the core-tube, and the coefficient of proportionality is a constant.

The use of equation (29) for the analysis of experimental data, however, may not be adequate for the following reasons. First of all, the surface thermal emissivity appearing in equation (29) is not a material constant, but is controlled strongly by the surface finish. Moreover, the thermal emissivity of a curved surface is usually difficult to measure. Accordingly, the expression may not be accurate if the coefficient is calculated from experimentally determined $\epsilon_1$ and $\epsilon_2$. Secondly, the Apollo 15 type drill core-tube has a spiral ridge on its outer surface, whose effect on the thermal radiative exchange area is too complex to be expressed in a mathematically rigorous form. Therefore, equation (29) needs to be modified if this effect is to be taken into account. Thirdly, neither the heater nor the core-tube are infinitely long as assumed in the derivation of equation (28), but have a finite length. In our experimental arrangement, the effect of finite axial extent may be important in the heater and core-tube system. We decided, therefore, to use an empirical formula to evaluate the heat transfer from the heater to the core-tube. As will be shown below, the theoretical expression (29) is useful in determining the functional form of the empirical formula.

The empirical formula was derived experimentally in the following way. An empty core-tube was placed in the core-sample position and the temperature variation due to heating was measured as a function of time at the surfaces of both the heater and core-tube. Since the core-tube is made of a thermally conductive alloy, the temperature difference across the core-tube wall can be assumed to be negligible unless the heating rate is exceedingly high. In that case, because the core-tube is empty, the heat inflow rate into the core-tube can be estimated from the increase in core-tube surface temperature as

$$Q = C \mathrm{d}(\delta T_1)/\mathrm{d}t, \tag{30}$$

where $C = \pi(b^2 - a^2)\, c_2 \rho_2$ is the heat capacity, per unit length of the core tube.

The above expression is to be equated with the empirical formula describing the heat inflow into the core-tube, the leading term of which is proportional to $\delta T_2 - \delta T_1$, as formula (29) suggests. Experimental data analysis showed, however, that the measured temperatures are more adequately

represented by an empirical formula if an additional term, proportional to $\delta T_1$, is included (figure 5). Thus,

$$Q = \eta(\delta T_2 - \delta T_1) + \nu \delta T_1, \tag{31}$$

where $\eta$ and $\nu$ are constants. If equations (30) and (31) are combined and integrated with respect to time the result will be

$$C\delta T_1(t) = \eta \int_0^t \{\delta T_2(\tau) - \delta T_1(\tau)\}\, \mathrm{d}\tau + \nu \int_0^t \delta T_1(\tau)\, \mathrm{d}\tau, \tag{32}$$

which enables $\eta$ and $\nu$ to be determined from temperatures $\delta T_1(t)$ and $\delta T_2(t)$ measured as a function of time $t$.

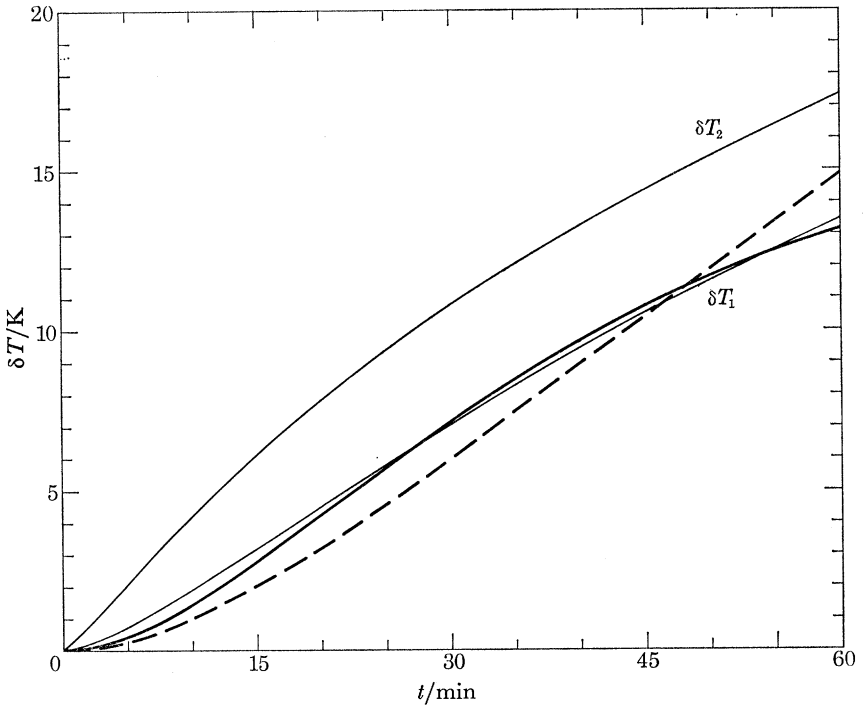


FIGURE 5. Variation of temperature measured as a function of time $t$, at the surfaces of the heater ($\delta T_2$) and the core-tube ($\delta T_1$) for a determination of the heat transmission characteristics. Heater, Al, h.a.; core-tube, (3) (see Table 1). Heater energized by a 27.5 V d.c. Measurement made at thermocouple position $L_2$. The digitized records are smoothed. Solid and dashed lines represent the theoretical best fit to the measured core-tube surface temperature, based, respectively, on formula (31) with and without the second term, i.e. ——, $Q = \eta(\delta T_2 - \delta T_1) + \nu \delta T_1$; – – –, $Q = \eta(\delta T_2 - \delta T_1)$.

The heating element currently in use for the Apollo 15 type drill-core sample measurements is composed of a coil of no. 30 Teflon coated constantan wire, wound uniformly over the core of the heater. The heater's total electrical resistance is 490 $\Omega$. Before the temperature measurements, the experimental heater and core-tube system was installed in a vacuum chamber and the atmospheric pressure within the chamber reduced to $10^{-4}$ Pa. This is to suppress gaseous convective motion which, if operative, will interfere with the radiative heat transfer. The heating element is energized by a constant d.c. voltage, either 25.0 or 27.5 V, for 60 min. The temperatures at the core-tube and heater surfaces are digitized and recorded at intervals of 1 min. These discrete values of temperature are used to determine $\eta$ and $\nu$ according to equation (32) by the least squares method.

During the development of the present thermal conductivity measurement technique, the heater's design was changed several times to improve the heat transmission characteristics between the heater and the core-tube. The reconstruction of the heater was also necessitated from the standpoint of lunar sample preservation. The heater, as originally constructed, was of stainless steel with its inner surface covered by a glossy chromic acid coating. The surface finish was later changed to a black nickel coating to render it radiatively diffuse with its thermal emissivity close to unity. Subsequently, to avoid exposing lunar material to the nickel compound, the heater was rebuilt from aluminium with a surface hard anodized by the use of stainless steel electrodes. The constants $\eta$ and $\nu$ of equation (31) were determined for each of these heaters, as shown in table 1, because they are necessary for the thermal conductivity test measurement.

TABLE 1. DETERMINATION OF HEAT TRANSMISSION CHARACTERISTICS FOR APOLLO 15 TYPE DRILL CORE TUBES AND TEST MEASUREMENTS OF THE THERMAL CONDUCTIVITY OF AN APOLLO 12 SIMULANT LUNAR SOIL SAMPLE

| | | heat transmission characteristics | | number of measurements, | sample bulk density | thermal conductivity | number of measurements, |
|---|---|---|---|---|---|---|---|
| | | $\eta$ | $\nu$ | | | | |
| heater† | core-tube‡ | $(10^{-2}\,\mathrm{W\,m^{-1}\,K^{-1}})$ | | $n'$ | $\rho_1/(\mathrm{g\,cm^{-3}})$ | $k_1/(10^{-3}\,\mathrm{W\,m^{-1}\,K^{-1}})$ | $n$ |
| s.s.c.a. | (1) | $27.0 \pm 1.2$ | $-(10.3 \pm 2.0)$ | 10 | 1.47 | $2.05 \pm 0.80$ | 7 |
| s.s.b.n. | (2) | $23.6 \pm 1.7$ | $-(14.3 \pm 1.5)$ | 13 | 1.58 | $2.29 \pm 0.86$ | 6 |
| s.s.b.n. | (2) | $33.0 \pm 3.7$ | $-(17.5 \pm 2.0)$ | 12 | 1.67 | $2.14 \pm 0.53$ | 3 |
| s.s.b.n. | (1) | 44.2§ | −16.2§ | — | 1.57 | $2.65 \pm 0.55$ | 10 |
| Al,h.a. | (3) | $38.0 \pm 5.4$ | $-(10.3 \pm 2.0)$ | 24 | 1.50 | $2.13 \pm 0.72$ | 21 |

† s.s.c.a.: stainless steel, chromic acid coating, inner radius $r_2 = 1.53$ cm, length $l = 15.24$ cm. s.s.b.n.: stainless steel, black nickel coating, $r_2 = 1.53$ cm, $l = 15.24$ cm. Al,h.a.: aluminium, hard anodized with stainless steel electrode, $r_2 = 1.78$ cm, $l = 20.32$ cm.

‡ Apollo 15 type drill core tube, outer radius $b = 1.165$ cm, inner radius $a = 1.020$ cm. (1), length $l = 38.74$ cm, weight $w = 161.9$ g, surface thermal emissivity $\epsilon_1 = 0.663$; (2), $l = 42.54$ cm, $w = 193.4$ g, $\epsilon_1 = 0.465$; (3), $l = 42.54$ cm, $w = 195.5$ g, $\epsilon_1 = 0.634$; (4) (not used for thermal conductivity test measurements), $l = 38.74$ cm, $w = 170.2$ g, $\epsilon_1 = 0.652$.

§ Estimated from surface thermal emissivity data.

The experimentally determined $\eta$ can be compared with the theoretically expected coefficient in equation (29). Surface thermal emissivity data are available for the heater and the core tube used in the test thermal conductivity measurement. Thermal emissivity of an aluminium specimen, with a flat surface finished by the same treatment as the heater, was measured by the Gier Dunkle double black body infrared reflectometer model DB100 giving a result of $\epsilon_2 = 0.934$, whereas that of the core-tube measured by the same instrument was $\epsilon_1 = 0.634$. When combined with the following parameters: $r_1 = 1.165$ cm, $r_2 = 1.778$ cm, $T_0 = 300$ K and $\sigma_b = 5.66961 \times 10^{-8}\,\mathrm{W\,m^{-2}\,K^{-4}}$, the constant becomes equal to $2.93 \times 10^{-1}\,\mathrm{W\,m^{-1}\,K^{-1}}$. As indicated in table 1, the experimentally determined value of $\eta$ is more than 35% higher than the theoretically expected value. This discrepancy may be due in part to the uncertain determination of thermal emissivity on the curved surface of the core tube and in part to the theory, which does not take into account the effect of the core-tube's spiral ridge on the radiative heat exchange between the heater and the core-tube.

*Numerical simulation of the experiment*

The values of $\nu$ listed in table 1 are all negative, indicating that the second term in empirical formula (31) represents the loss of heat to the axial direction of the core-tube. There are two

mechanisms to account for the axial dissipation of heat: (1) thermal conduction through the wall of the metallic core-tube, and (2) radiation from the surface of the core-tube. The latter consists of two components, one from the outer surface of the core-tube into the solid angles not subtended by the inner wall of the heater; and the other from the inner surface of the empty core-tube towards the upper and lower ends of the core-tube. In the latter component of radiative heat transfer, the path of a thermal radiative ray, emitted from the inner surface of the core-tube is not straightforward, but subject to a complex reverberation. It is obvious that this mode of heat transfer, effective when the core-tube is empty, is effectively suppressed when the core-tube is filled with a radiatively opaque sample. The applicability of formula (31) to the thermal conductivity measurements depends, therefore, on the evaluation of this effect. The coefficients in the formula derived from the measurement on an empty core-tube are valid for a sample filled core-tube, only when the effect is negligible.

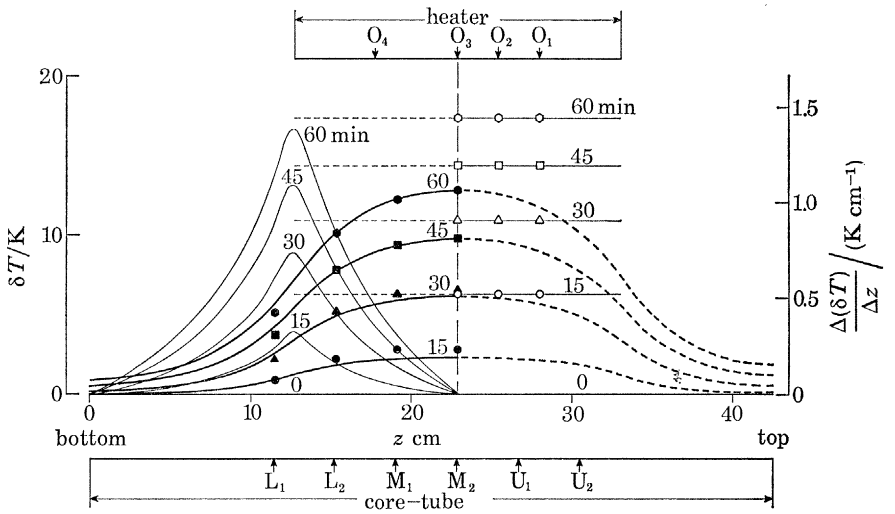


FIGURE 6. Numerical simulation of an empty core-tube experiment. Calculated temperatures are shown with temperature measurement data for a determination of the heat transmission characteristics. Open symbols: measured heater surface temperatures. Closed symbols: measured core tube surface temperatures. Thin straight lines: theoretical heater surface temperatures equal to the temperatures measured at the middle of the heater. Bold curved lines: calculated core-tube surface temperatures. Thin curved lines: core tube surface temperature gradient in the direction of the core tube's axis.

Evaluation of the effect of axial heat loss was made by a numerical method. Solving the heat transfer equation numerically, with the aid of a finite difference technique, simulated the experiment of heating an empty core-tube. To compare with the numerical result, temperature measurements were made by using all thermocouples attached to the heater and core-tube with the same relative position of the heater to the core-tube assumed in the simulation. The data showed that the temperatures, as a function of time measured on the inner surface of the heater, were nearly identical regardless of the position of the thermocouples. The heater's inner surface was therefore assumed to be isothermal and equal to the temperature measured at the middle of the heater. Thermal radiation was assumed to be the mode of heat exchange between the heater and the core-tube while thermal conduction along the core-tube and radiation outside and inside the core-tube were the modes of heat dissipation. The necessary values of thermal emissivity for the heater and the core-tube's outer surface were taken from direct measurement data by an infrared reflectometer. The core-tube's inner surface was assumed to have the same

thermal emissivity as its outer surface. The heater and core-tube were approximated by a set of concentric isothermal annuli of axial length $\Delta z < 1$ cm, and the temperature development with time, for each of the annuli representing the core-tube, was calculated explicitly for the time interval $\Delta t = 5$ s. The solution of the finite difference equation was stable for the choices of space and time intervals as indicated above.

Figure 6 summarizes the results of the calculation. The calculated core-tube temperatures, together with the measured temperatures, are shown for 15, 30, 45 and 60 min after the start of heating. The generally excellent agreement between calculation and measurement indicates that the numerical modelling of the experiment was appropriate. Another calculation was made in which the core-tube's inner surface thermal emissivity was assumed to be zero, corresponding to the assumption that the radiative heat transfer inside the core-tube is totally suppressed. A comparison of the results showed that the calculated temperature at the core-tube's surface was higher for the latter, but the difference never exceeded 1 %, indicating that the effect of radiative heat transfer inside the core-tube contributes no more than 1 % to the heat loss in the axial direction of the core-tube. It can be concluded that no substantial error will be incurred in applying expression (31), with numerical coefficients determined from an empty core-tube measurement, to the thermal conductivity determination of a sample filled core-tube.

Other important experimental features can be seen in figure 6. To illustrate the amount of heat loss in the axial direction of the core-tube, the gradient of the core-tube surface temperature in the direction of its axis is indicated on the figure. It is remarkable that the locus of maximum heat loss coincides with the heater's position. Although only the lower half of the core-tube temperature distribution is shown in the figure, the same is true of the upper half. Heat dissipation in the axial direction of the core-tube becomes null at the middle of the heater because the core-tube's temperature distribution is symmetrical, with the plane of symmetry passing through the heater's centre and is perpendicular to the core-tube's axis.

The thermal conduction equation necessary for the experiment was solved for a composite circular cylinder of infinite axial extent. However, the solution is also valid for a finite axial extent, $|z| \leqslant h$, provided that the boundaries, $z = \pm h$ are insulating so that the direction of axially symmetric heat flow in the region $|z| < h$ is confined in a plane perpendicular to the cylinder's axis. The numerical simulation of the experiment showed, however, that the locus of the null heat loss is restricted to a point at the middle of the heater, indicating that the two dimensional thermal conduction assumption holds only for the narrow section of the core-tube containing the plane of symmetry. Outside the section, the heat flow is no longer confined within a plane perpendicular to the core-tube's axis but has a component parallel to it. The situation will be the same when the core-tube is filled with a sample, because the temperature distribution in the sample must also be symmetrical with respect to the same plane of symmetry unless the sample material is inhomogeneous or anisotropic.

In the present experimental arrangement, to measure thermal conductivity, it is important to place the centre of the heater precisely at the spot of thermal conductivity determination where the core-tube temperature sensor is attached. If the core-tube surface temperature is measured away from the middle of the heater, the component of heat flow, parallel to the direction of the core-tube's axis, will not be negligible, thereby invalidating the thermal conductivity determination theory because it assumes a thermal conduction in a cylindrical system with its flow line confined within a plane perpendicular to the cylindrical axis. Similarly, an empty core-tube measurement must be made with the heater centred at the very spot of the


PHILOSOPHICAL TRANSACTIONS OF THE ROYAL SOCIETY A MATHEMATICAL, PHYSICAL & ENGINEERING SCIENCES

core-tube's surface temperature measurement. If there is a component of heat flow parallel to the core-tube axis at the spot where the core-tube surface temperature is measured, the empirical formula (31), with numerical coefficients thus determined, will not give a correct amount of heat inflow into the core-tube as the theory requires.

## Thermal conductivity test measurement

Since the present technique of thermal conductivity measurement is new, we considered it necessary to demonstrate its feasibility by making a test measurement. The core-tubes whose heat transmission characteristics had been determined, were filled with a terrestrial analogue of the lunar material and its thermal conductivity was measured by using the present technique. This result was compared with the conductivity of the same material measured by another technique considered standard.

Table 2. Grain size distribution of an Apollo 12 simulant lunar soil sample

| material | grain size range/mm | percentage weight fraction |
|---|---|---|
| Knippa basalt | 1.68–(5.0) | 5 |
| | 0.297–1.68 | 16 |
| | 0.149–0.297 | 13 |
| | 0.074–0.149 | 16 |
| Berkeley basalt | 0.050–0.074 | 7.2 |
| | 0.027–0.050 | 13.4 |
| | 0.016–0.027 | 13.8 |
| | 0.0085–0.016 | 7.5 |
| | 0.0044–0.0085 | 4.4 |
| | (0.0010)–0.0044 | 3.7 |

### *Sample*

The terrestrial analogue of the lunar material used for this study is an Apollo 12 simulant lunar soil, prepared by W. D. Carrier of the Johnson Space Center, N.A.S.A. This consists of a mixture of powdered Berkeley and Knippa basalts with grain size distribution (table 2) similar to that of Apollo 12 lunar soil samples (Scott *et al.* 1971). It has been shown that the grain size distributions of soil samples from subsequent Apollo missions are not significantly different from those of the Apollo 12 samples (Mitchell *et al.* 1972; Carrier *et al.* 1973). Accordingly, the use of this particular terrestrial analogue is adequate in a lunar sample simulation study.

### *Reduction of the sample's interstitial gaseous pressure*

The thermal conductivity of a particulate material, such as the lunar soil simulant, is known to decrease substantially as the pressure of gas filling the interstices of the material is reduced from $1.01 \times 10^5$ Pa to 0.1 Pa. Below 0.1 Pa however, it becomes insensitive to the change of the interstitial gaseous pressure (Wechsler & Glaser 1965). Accordingly, to simulate the lunar surface condition, the sample's interstitial gaseous pressure must be kept below 0.1 Pa during the measurement. It was necessary to suppress the convective motion of the gas outside the core-tube to keep it from interfering with the radiative heat transfer from the heater to the core-tube. The gaseous pressure inside the core tube needs also to be kept as low as the outside.

The Apollo 15 type drill-core samples are sealed at their lower end by a cap and at the upper end by a plug inserted into the core-tube. The plug is a piece of Teflon fitting tightly inside the inner wall of the core-tube, thereby rendering it airtight. To facilitate the reduction of gaseous pressure within the core-tube, permission was obtained from N.A.S.A.'s Lunar Sample Curator to replace the plug before the thermal conductivity measurement. This new plug, made of Teflon, has the same outer dimensions as the old one, but has a hole 10 mm in diameter along its axis serving as a conduit connecting the inside of the core-tube to the outside. To the plug's lower end, under the hole, is affixed a Bendix poroplate stainless steel screen with a mesh of 5 μm. The lunar regolith material contains particles finer than 5 μm (Gold *et al.* 1971; Görz *et al.* 1972; King *et al.* 1972). Since, however, the mass fraction of these fine particles seldom exceeds 1 % of the total material, the use of the screen is effective in preventing any significant leakage of the lunar soil particles.

The same cap and plug, prepared for the lunar sample study, were used during the test measurement. Great care was taken to control the rate of reducing the gaseous pressure in the chamber containing the core-tube filled with test material. A rapid change in gaseous pressure outside the core-tube should induce a large gradient in gaseous pressure within the core-tube, which could result in a catastrophic dislocation of the sample as well as a leakage of particles finer than the screen mesh.

Experimental pumping was repeated to determine an optimum pumping rate. In one experiment, a sample of fluorescent $CaWO_4$, powdered finer than 2 μm, was placed on top of the lunar simulant material to see if the selected pumping rate caused any significant diffusion of the material. A methyl cellulose millipore filter with a pore size of 0.22 μm was placed on the downstream side of the screen, and, after the experiment, examined by electron microscope to detect any $CaWO_4$ particles. At the same time, the upper portion of the core-tube in the vicinity of the plug was scanned by radiation from a long-wave ultraviolet source to reveal any trace of fluorescence. In another experiment, with the use of powdered silica glass, artificial layers were embedded in the lunar simulant soil sample and the sample examined by X-rays taken before and after the experiments to indicate any disturbances incurred in the artificial stratification. Later, the same experiment was repeated with a glass tube of the same length and inner diameter as the lunar core-tube to visually examine the artificial strata for possible disturbances. On the basis of these experiments, we conclude that, providing the rate of pumping does not exceed $2\,\mathrm{Pa\,s^{-1}}$ while the gas pressure in the vacuum chamber is reduced from $1.01 \times 10^5$ Pa to less than $10^2$ Pa, the texture of the lunar sample in the core-tube will remain unaltered. We also inferred that the same rate must be maintained when the pressure in the chamber is restored from less than $10^2$ Pa to $1.01 \times 10^5$ Pa after the thermal conductivity measurement.

The above pumping criteria were adopted for the thermal conductivity test measurements. A needle valve is essential in our vacuum equipment to maintain an extremely slow rate of pumping and its fine adjustment. A brief description is appropriate here with regard to the vacuum equipment. Our original vacuum equipment consisted of an oil sealed rotary pump and a diffusion pump. These were later replaced by a combination of sorption and sputter ion pumps to avoid an oil leakage into the vacuum chamber to protect the lunar material against chemical contamination. For this reason, stainless steel tubings and bellows were used in place of copper and rubber tubings, and aluminium gaskets instead of copper in our oil-less vacuum apparatus. A high vacuum is easily produced with the apparatus currently in use. The air pressure in the vacuum chamber stays around $10^{-5}$ Pa during the determination of heat trans-

mission characteristics but is a little higher, $10^{-3}$–$10^{-4}$ Pa, during the test measurement of the thermal conductivity, owing to the degassing of the sample material.

*Thermal conductivity determination*

The procedure followed during thermal conductivity measurements is the same as for the determination of heat transmission characteristics. From the discrete values of measured temperatures $\delta T_1(t_j)$ and $\delta T_2(t_j)$ $(j = 1, 2, \ldots, j_{\max})$, the heat inflow into the core-tube $Q(t_j)$ is calculated from formula (31) in which the numerical coefficients, $\eta$ and $\nu$, have been determined by a measurement on the empty core-tube. The theoretical temperature at the surface of the core-tube $v_2(t_j)$ is, then, computed according to formula (27), where it will be recalled that $-2b\pi F_i = \frac{1}{2}(Q(t_i) + Q(t_{i-1}))$ and $i_{\max} = j$. Of the constants appearing in equation (27), the inner and outer radii of the core-tube are known, as well as the density ($\rho_2 = 4.43\,\mathrm{g\,cm^{-3}}$) and the specific heat ($c_2 = 0.530\,\mathrm{J\,g^{-1}\,K^{-1}}$ at 300 K) for the titanium alloy Ti–6Al–4V of which the Apollo 15 type drill core-tube is made. For the Apollo 12 simulant lunar soil sample, a specific heat, $c_1 = 0.715\,\mathrm{J\,g^{-1}\,K^{-1}}$, was assumed and the bulk density $\rho_1$ was calculated from the sample's mass and volume for each experiment (table 1). The theoretical core-tube surface temperature $v_2(t_j)$ is, then, a function of the sample's thermal conductivity. The trial $k_1$ was adjusted by an electronic computer to minimize the sum of the squared residuals between the calculated and the measured temperatures.

$$\sum_{j=1}^{j_{\max}} \{v_2(t_j) - \delta T_1(t_j)\}^2 = \min. \tag{33}$$

The results are shown in table 1.

TABLE 3. THERMAL CONDUCTIVITY OF AN APOLLO 12 SIMULANT LUNAR SOIL SAMPLE MEASURED BY THE DIFFERENTIAL LINE HEAT SOURCE TECHNIQUE UNDER AN INTERSTITIAL GASEOUS PRESSURE OF $10^{-5}$ Pa

Original data (Fountain & West 1975) interpolated to 300 K.

| sample bulk density/($\mathrm{g\,cm^{-3}}$) | thermal conductivity/($10^{-3}\,\mathrm{W\,m^{-1}\,K^{-1}}$) |
|---|---|
| 1.25 | 1.58 |
| 1.50 | 1.61 |
| 1.75 | 2.89 |
| 1.80 | 5.08 |

The standard values of thermal conductivity were determined at the Marshall Space Flight Center, N.A.S.A. (Fountain & West 1975) by means of a differential line heat source technique developed by Scott *et al.* (1973). The original study gives the thermal conductivity of Apollo 12 simulant soil samples as a function of the bulk density and temperature under a vacuum of $10^{-5}$ Pa. The values interpolated at 300 K are reproduced in table 3. The tables shows that the conductivity, determined by the line heat source technique, varies from 1.61 to $2.89 \times 10^{-3}\,\mathrm{W\,m^{-1}\,K^{-1}}$ as the sample's density increases from 1.50 to 1.75 g $\mathrm{cm^{-3}}$. This agrees favourably with our measurements of $2.05$–$2.65 \times 10^{-3}\,\mathrm{W\,m^{-1}\,K^{-1}}$ for a density ranging from 1.47 to 1.67 $\mathrm{g\,cm^{-3}}$, demonstrating the validity of the new technique.

Figure 7 is an example of a temperature record. In this particular measurement, the heater was energized by a d.c. voltage of 27.5 V. The rate of heat generation per unit length of the heater is, therefore, $0.921\,\mathrm{W\,m^{-1}}$. For this rate of heat generation, the increases of the heater and the core-tube surface temperatures are, respectively, 16.5 and 10.8 K, after 60 min of




PHILOSOPHICAL TRANSACTIONS OF THE ROYAL SOCIETY A MATHEMATICAL, PHYSICAL & ENGINEERING SCIENCES

heating. This implies that the temperature disturbance to the sample, due to the thermal conductivity measurement, was kept within 11 K. Unless the thermal conductivity of lunar core samples is substantially lower than that of the Apollo 12 simulant lunar soil, the maximum temperature disturbance to the sample, by the present thermal conductivity technique, will remain the same order of magnitude. This is one of the advantages of the technique fitting the requirements of lunar sample preservation.

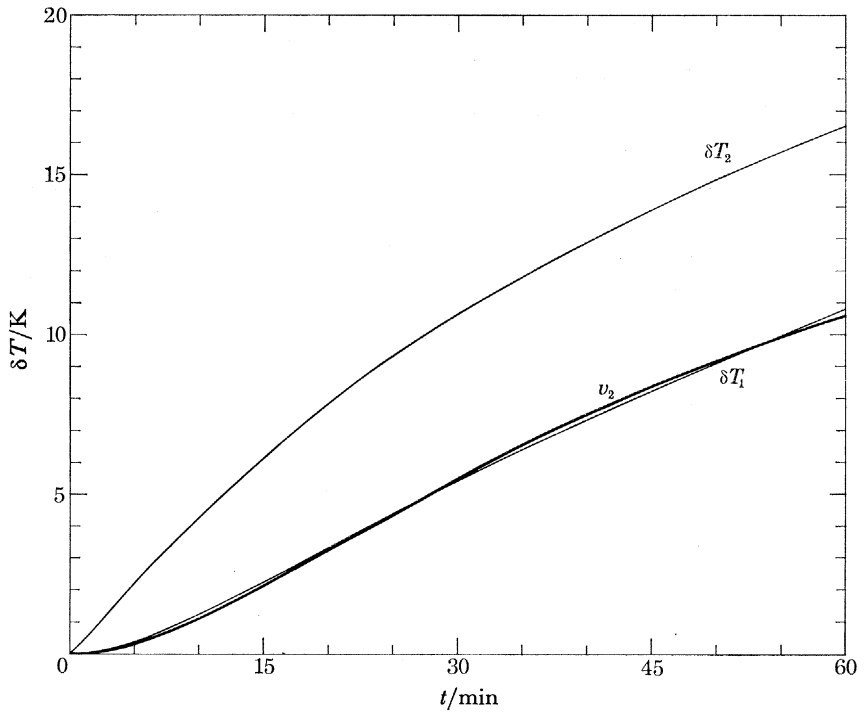


FIGURE 7. Temperature variation measured as a function of time $t$, at the heater surfaces ($\delta T_2$) and the core-tube ($\delta T_1$) for a determination of the thermal conductivity of an Apollo 12 simulant lunar soil sample with a bulk density of 1.50 g cm$^{-3}$ contained in test core-tube (3). Heater Al, h.a., energized by a 27.5 V d.c. The experiment was made at the thermocouple's position $M_1$. The digitized records are smoothed. The solid line represents the theoretical best fit to the measured core-tube surface temperature calculated from formula (27).

The values of thermal conductivity and their uncertainties given in table 1 are the averages and standard deviations calculated from the result of repeated measurements. For the number of determinations, $n$, varying from 3 to 21, the standard deviations are 20–40 % of the averages. They are certainly large. It may be questioned whether the large uncertainty associated with the conductivity determination is inherent in the method of measurement presented in this paper.

It must be noted that the thermal conductivity of the lunar simulant soil sample under vacuum, as reported above, is as low as that of common commercial thermal insulators. This enabled us to regard the core-tube as a perfect thermal conductor and to use the simplified solution of the thermal conduction equation for the data analysis. Undoubtedly, however, the large thermal conductivity contrast between the sample and the core-tube enhanced the difficulty of measurement. For a sample with an exceedingly low thermal conductivity, the core-tube surface temperature may not be controlled sensitively by the sample's thermal conductivity because the heat transmitted from the heater to the core-tube does not flow effectively into the sample. The core-tube surface temperature is controlled more sensitively by the axial heat loss through the

conductive core-tube. As a consequence, a small error in the temperature measurement would result in a large difference in the determined value of the sample's thermal conductivity. The resolution of the thermal conductivity determination by the present technique is expected to improve as the sample's thermal conductivity increases. The best resolution will probably be obtained when the sample's thermal conductivity is of the same order of magnitude as that of the core-tube.

## Lunar core sample measurements

The measurement method thus established was utilized to determine the thermal conductivity of lunar core samples. So far, measurements have been completed on two Apollo 17 drill core samples, 70002 and 70006, the two sections of the deep drill string collected from depths of 280–317 cm and 120–160 cm respectively at the Apollo 17 landing site about 40 m north of the Apollo Lunar Surface Experiment Package's central station. The length of the standard Apollo 15 type drill core-tube containing sample 70006 is 42.54 cm. However, the core-tube of sample 70002 is only 39.54 cm long because it is the lowest section of the string attached directly to the drilling bit. The joint length is 2.54 cm of the core-tubes so that the remaining 37.0 cm for sample 70002 and 40.0 cm for sample 70006, shown by X-rays to be completely filled with lunar regolith material, are suitable for the thermal conductivity measurements.

As originally conceived, it was intended only to make measurements of the thermal conductivity at one spot near the middle of the core-tube. With the installation of the screw rod and mechanical feedthrough, it became possible to determine the thermal conductivity at several locations along the entire length of the core tube. Six thermocouples, labelled respectively $L_1$, $L_2$, $M_1$, $M_2$, $U_1$ and $U_2$, were attached to the core tube, the lowest, $L_1$, 11.43 cm from the lower end of the core tube while the others were separated by 3.81 cm. Four thermocouples, $O_1$, $O_2$, $O_3$ and $O_4$, are attached to the heater at 5.08, 7.62, 10.16 and 15.24 cm respectively from the upper end of the heater (see figure 6). As the heater is 20.32 cm long, thermocouple $O_3$ is equidistant from the upper and lower ends of the heater. To determine the thermal conductivity at one of the core-tube's thermocouple positions, the heater position is adjusted so that thermocouple $O_3$ is at the same level as the core-tube's thermocouple at which the thermal conductivity is to be determined. For sample 70006, contained in a standard Apollo 15 type drill core-tube, thermal conductivity determinations were possible at the core-tube thermocouple positions $L_2$, $M_1$, $M_2$ and $U_1$ because, in the present experimental arrangement, the heater cannot be brought to the positions of thermocouples $L_1$ and $U_2$. Because of its shorter length, the thermal conductivity of core-tube 70002 could only be determined at thermocouples $L_2$, $M_1$ and $M_2$.

To determine the thermal conductivity from the temperature data, the sample's bulk density and specific heat must be known. The bulk density values were taken from Mitchell *et al.* (1973); namely, 1.74 g cm$^{-3}$ for sample 70002 and 1.80 g cm$^{-3}$ for sample 70006. No specific heat data have been reported for Apollo 17 lunar samples. Measurements on various lunar materials comprising soils, breccias and basalts from other Apollo missions (Hemingway *et al.* 1973; Robie & Hemingway 1971; Robie *et al.* 1970) showed that the variation of specific heat as a function of temperature is relatively small from sample to sample. At 300 K, the average specific heat of four soil samples was $0.765 \pm 0.017$ J g$^{-1}$ K$^{-1}$, whereas an average of all nine samples was $0.761 \pm 0.016$ J g$^{-1}$ K$^{-1}$. Since the lunar regolith material consists of a mixture of soil and solid rock fragments, the latter will be a more appropriate estimate of the lunar regolith specific heat. It is reasonable to assume that the specific heat of Apollo 17 lunar core samples is not significantly

different from that of the lunar materials from preceding missions. The specific heat value of $0.761\,J\,g^{-1}\,K^{-1}$ was used in the thermal conductivity calculations. In the previous section, we assumed that the Apollo 12 simulant lunar soil has the same specific heat as the lunar soil, or $0.765\,J\,g^{-1}\,K^{-1}$.

TABLE 4. THERMAL CONDUCTIVITY OF TWO APOLLO 17 DRILL CORE SAMPLES, 70002 AND 70006

| sample density, $\rho_1$ (g cm$^{-3}$) specific heat, $c_1$ (J g$^{-1}$ K$^{-1}$) | thermocouple position | thermal conductivity $k_1/(10^{-3}\,W\,m^{-1}\,K^{-1})$ | number of measurements, $n$ |
|---|---|---|---|
| 70006 | | | |
| $\rho_1 = 1.80$ | $U_1$ | $4.88 \pm 1.46$ | 13 |
| $c_1 = 0.765$ | $M_1$ | $4.84 \pm 2.42$ | 10 |
| | $M_1$ | $3.87 \pm 2.66$ | 15 |
| | $L_2$ | $4.23 \pm 0.51$ | 14 |
| 70002 | | | |
| $\rho_1 = 1.74$ | $M_2$ | $3.48 \pm 0.43$ | 8 |
| $c_1 = 0.765$ | $M_1$ | $2.02 \pm 0.34$ | 8 |
| | $L_2$ | $1.88 \pm 0.41$ | 8 |

In table 4, a summary of the measurement results, the values of the thermal conductivity for samples 70002 and 70006 are shown to be $1.9$–$4.9 \times 10^{-3}\,W\,m^{-1}\,K^{-1}$ at around 300 K. They are intermediate between the thermal conductivity of the lunar regolith as determined *in situ* and that of the lunar soil samples measured in the laboratory, indicating that the discrepancy between the two types of measurement has not been fully confirmed by the lunar core sample measurements. It must be inquired why the thermal conductivity of the lunar core samples is not as high as that of the lunar regolith as determined *in situ*. It will be necessary to study in detail the effects of the sampling procedure, in particular any processes which may alter the intergranular thermal contact of the lunar regolith material, on the thermal conductivity of lunar core samples. A detailed discussion of the results obtained above, as well as a possible interpretation of the higher thermal conductivity of the lunar regolith, will be given elsewhere.

## CONCLUSIONS

The new thermal conductivity measurement technique, presented in this paper, can be applied to any terrestrial or planetary material sampled in a cylindrical container. In our application of the method to the lunar core samples, the thermal conductivity was deduced from the temperature data by using the simplified solution (27) in which the thermal conductivity of the container was assumed to be infinite. This assumption is justifiable because the lunar regolith samples were, as shown in table 4, $10^{-3}$ times less conductive than the core-tube alloy. For the case in which the sample is as conductive as its container, the solution for a finite container conductivity can be used to reduce the temperature data. Solution (9), obtained for a constant heat flux, can be modified easily for a time varying heat flux in the same way as expression (27) was derived from solution (20).

The numerical process employed in the determination of the thermal conductivity becomes more complicated for the case of a finite container conductivity. As seen from equation (19), the constants $\alpha_s$ appearing in the simplified solution (20) are independent of the sample's thermal conductivity, $k_1$. Accordingly, once equation (19) has been solved for $\alpha_s$, the same $\alpha_s$ can be used for a different $k_1$ to compute the corresponding theoretical core-tube surface temperature, $v_2$,

provided that the sample's density, $\rho_1$, and its specific heat, $c_1$, remain unchanged. When the thermal conductivity of the container is finite, the constants $\alpha_s$ in solution (9) are determined from equation (12), which contains $k_1$ parametrically as well as $\rho_1$ and $c_1$. Therefore, the constants $\alpha_s$ must be recalculated for each trial of $k_1$.

It is possible, though rather uncommon, for a sample of unknown thermal conductivity to be contained in a spherical or disk shaped container. The thermal conductivity of these samples can be determined by the same principle as that applied to the samples in a cylindrical container. The necessary solutions for the thermal conduction equations for these measurements are given in the two appendixes of this paper.

## Appendix A. Derivation of the solution for the thermal conduction equation of the composite circular cylinder

The Laplace transform method, described in detail in Carslaw & Jaeger (1959), was utilized to solve the thermal conduction equations presented in the text. The outline of the solution derivation will be given.

Take the Laplace transform of $v_1$ and $v_2$,

$$\bar{v}_1 = \int_0^\infty e^{-pt} v_1 \, dt \quad \text{and} \quad \bar{v}_2 = \int_0^\infty e^{-pt} v_2 \, dt. \tag{A 1}$$

Equations (1) and (2) are converted to the subsidiary equations

$$(d^2/dr^2 + (1/r)\, d/dr - q_1^2)\, \bar{v}_1 = 0, \tag{A 2}$$

$$(d^2/dr^2 + (1/r)\, d/dr - q_2^2)\, \bar{v}_2 = 0, \tag{A 3}$$

where

$$q_1^2 = p/\kappa_1 \quad \text{and} \quad q_2^2 = p/\kappa_2, \tag{A 4}$$

and $p$ is the transformed time variable. The subsidiary initial and boundary conditions are

$$k_2 (d\bar{v}_2/dr) = -F_0/p, \quad r = b, \tag{A 5}$$

$$\bar{v}_1 = \bar{v}_2, \quad r = a, \tag{A 6}$$

$$k_1 (d\bar{v}_1/dr) = k_2 (d\bar{v}_2/dr), \quad r = a, \tag{A 7}$$

$$(d\bar{v}_1/dr) = 0, \quad r = 0. \tag{A 8}$$

The general solutions of (A 2) and (A 3) are given in terms of the modified Bessel functions. The solution for (A 2) satisfying (A 8) is

$$\bar{v}_1 = A_1 I_0(q_1 r), \tag{A 9}$$

and the general solution for (A 3) is

$$\bar{v}_2 = A_2 I_0(q_2 r) + B_2 K_0(q_2 r). \tag{A 10}$$

The coefficients $A_1$, $A_2$, and $B_2$ in (A 9) and (A 10) are determined by (A 5), (A 6), and (A 7). The equation

$$\begin{bmatrix} 0 & k_2 q_2 I_1(q_2 b) & -k_2 q_2 K_1(q_2 b) \\ I_0(q_1 a) & -I_0(q_2 a) & -K_0(q_2 a) \\ k_1 q_1 I_1(q_1 a) & -k_2 q_2 I_1(q_2 a) & k_2 q_2 K_1(q_2 a) \end{bmatrix} \begin{bmatrix} A_1 \\ A_2 \\ B_2 \end{bmatrix} = \begin{bmatrix} -F_0/p \\ 0 \\ 0 \end{bmatrix} \tag{A 11}$$

leads to the solutions

$$A_1 = -F_0/pq_2a\,\Delta(p), \tag{A 12}$$

$$A_2 = \frac{-F_0}{p\Delta(p)}\left\{I_0(q_1a)\,K_1(q_2a) + \frac{k_1}{k_2\kappa}I_1(q_1a)\,K_0(q_2a)\right\}, \tag{A 13}$$

$$B_2 = \frac{-F_0}{p\Delta(p)}\left\{I_0(q_1a)\,I_1(q_2a) - \frac{k_1}{k_2\kappa}I_1(q_1a)\,I_0(q_2a)\right\}, \tag{A 14}$$

where

$$\kappa = \sqrt{(\kappa_1/\kappa_2)} \tag{A 15}$$

and

$$\begin{aligned}\Delta(p) = {} & I_1(q_2b)\{q_1k_1I_1(q_1a)\,K_0(q_2a) + q_2k_2I_0(q_1a)\,K_1(q_2a)\} \\ & + K_1(q_2b)\{q_1k_1I_1(q_1a)\,I_0(q_2a) - q_2k_2I_0(q_1a)\,I_1(q_2a)\}.\end{aligned} \tag{A 16}$$

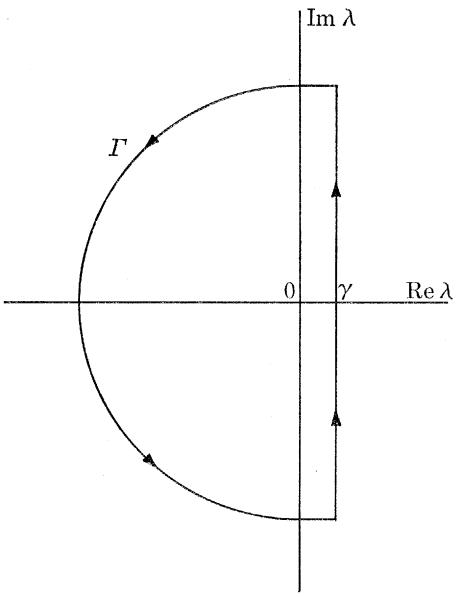


FIGURE A 1. Path of the contour integration on the complex λ-plane.

From $\bar{v}_1$ and $\bar{v}_2$ thus determined, $v_1$ and $v_2$ are obtained by the inverse Laplace transform

$$v_1 = \frac{1}{2\pi i}\int_{\gamma-i\infty}^{\gamma+i\infty} e^{\lambda t}\,\bar{v}_1(\lambda)\,d\lambda \quad \text{and} \quad v_2 = \frac{1}{2\pi i}\int_{\gamma-i\infty}^{\gamma+i\infty} e^{\lambda t}\,\bar{v}_2(\lambda)\,d\lambda, \tag{A 17}$$

where

$$\bar{v}_1(\lambda) = A_1(\lambda)\,I_0(\mu_1 r) \tag{A 18}$$

and

$$\bar{v}_2(\lambda) = A_2(\lambda)\,I_0(\mu_2 r) + B_2(\lambda)\,K_0(\mu_2 r). \tag{A 19}$$

In (A 18) and (A 19)

$$\mu_1 = \sqrt{(\lambda/\kappa_1)} \quad \text{and} \quad \mu_2 = \sqrt{(\lambda/\kappa_2)}, \tag{A 20}$$

and by writing $A_1(\lambda)$, $A_2(\lambda)$ and $B_2(\lambda)$ we emphasize that in (A 12), (A 13) and (A 14) the parameter $p$ has been replaced by a complex variable $\lambda$.

It can be shown that the integrals (A 17) are equivalent to the contour integrals on the complex $\lambda$ plane along a closed path shown in figure A 1 with $\gamma > 0$ and the radius of the semicircle $\Gamma$ tending to infinity. Accordingly the integrals are evaluated by the sum of the residues at the poles of the integrands enclosed in the contour.

It is noted that the integrands of the inverse transforms (17) are single value functions of the complex variable $\lambda$ with a double pole at $\lambda = 0$ and single poles at $\lambda = -\kappa_1 \alpha_s^2$ where $\alpha_s$, $s = 1, 2, \ldots$ are the positive roots of

$$\Delta(\lambda) = \Delta(-\kappa_1 \alpha^2) = 0 \tag{A 21}$$

for $\alpha$. An explicit expression of (A 21) is given in (12).

We will first evaluate $v_1$. Rewriting (A 18) as

$$\bar{v}_1 = A_1(\lambda)\, I_0(\mu_1 r) = \frac{-F_0}{\lambda \Delta(\lambda)} \frac{I_0(\mu_1 r)}{\mu_1 a} = \frac{f(\lambda)}{\lambda^2 D(\lambda)}, \tag{A 22}$$

we define

$$f(\lambda) = -F_0 \frac{\kappa_2^{\frac{1}{2}}}{a} I_0(\mu_1 r), \tag{A 23}$$

$$D(\lambda) = \Delta(\lambda)/\lambda^{\frac{1}{2}}. \tag{A 24}$$

Then the residue at $\lambda = 0$ becomes

$$\begin{aligned} \operatorname{Res}(e^{\lambda t} \bar{v}_1)_{\lambda=0} &= [(d/d\lambda)\{e^{\lambda t} f(\lambda)/D(\lambda)\}]_{\lambda=0} \\ &= \frac{f(0)}{D(0)} \left\{ t + \frac{f'(0)}{f(0)} - \frac{D'(0)}{D(0)} \right\}, \end{aligned} \tag{A 25}$$

where, from (A 23),

$$f(0) = -F_0(\kappa_2^{\frac{1}{2}}/a), \tag{A 26}$$

$$f'(0) = -F_0(\kappa_2^{\frac{1}{2}}/a)\,(r^2/4\kappa_1), \tag{A 27}$$

and from (A 24)

$$D(0) = \tfrac{1}{2}(\kappa_2^{\frac{1}{2}}/ab) \left\{ \frac{k_1}{\kappa_1} a^2 + \frac{k_2}{\kappa_2} (b^2 - a^2) \right\}, \tag{A 28}$$

$$\begin{aligned} D'(0) = \tfrac{1}{8}(a^2/\kappa_2^{\frac{1}{2}}) \Bigg[ \frac{k_1}{\kappa_1} \left\{ \frac{\kappa_2}{2\kappa_1} \frac{a}{b} + \frac{2b}{a} \ln \frac{b}{a} - \left( \frac{b}{a} - \frac{a}{b} \right) \right\} \\ + \frac{k_2}{\kappa_2} \left\{ \frac{\kappa_2}{\kappa_1} \left( \frac{b}{a} - \frac{a}{b} \right) + \frac{1}{2} \left( \frac{b^3}{a^3} - \frac{a}{b} \right) - \frac{2b}{a} \ln \frac{b}{a} \right\} \Bigg]. \end{aligned} \tag{A 29}$$

The residue at $\lambda = -\kappa_1 \alpha_s^2$ is

$$\begin{aligned} \operatorname{Res}(e^{\lambda t} \bar{v}_1)_{\lambda=-\kappa_1 \alpha_s^2} &= [e^{\lambda t} f(\lambda)/(d/d\lambda)\{\lambda^2 D(\lambda)\}]_{\lambda=-\kappa_1 \alpha_s^2} \\ &= e^{-\kappa_1 \alpha_s^2 t} f(-\kappa_1 \alpha_s^2)\, \Phi(\alpha_s), \end{aligned} \tag{A 30}$$

where

$$\Phi(\alpha_s) = 1/[(d/d\lambda)\{\lambda^2 D(\lambda)\}]_{\lambda=-\kappa_1 \alpha_s^2} \tag{A 31}$$

As

$$f(-\kappa_1 \alpha_s^2) = -F_0(\kappa_2^{\frac{1}{2}}/a)\, J_0(r\alpha_s), \tag{A 32}$$

we put

$$\Psi(\alpha_s) = \Phi(\alpha_s)/(2ab/\kappa_2^{\frac{1}{2}}), \tag{A 33}$$

so that (A 30) becomes

$$\operatorname{Res}(e_\lambda{}^t \bar{v}_1)_{\lambda=-\kappa_1 \alpha_s^2} = 2bF_0\, e^{-\kappa_1 \alpha_s^2 t} J_0(r\alpha_s)\, \Psi(\alpha_s). \tag{A 34}$$

An explicit expression for (A 33) is given in (11).

From (A 25) and (A 34) we obtain

$$v_1 = \operatorname{Res}(e^{\lambda t} \bar{v}_1)_{\lambda=0} + \sum_{s=1}^{\infty} \operatorname{Res}(e^{\lambda t} \bar{v}_1)_{\lambda=-\kappa_1 \alpha_s^2}, \tag{A 35}$$

as explicitly given in (8).

The evaluation for $v_2$ is similar. With $D(\lambda)$ defined in (A 24), (A 19) can be rewritten as

$$v_2 = A_2(\lambda)\, I_0(\mu_2 r) + B_2(\lambda)\, K_0(\mu_2 r) = g(\lambda)/\lambda^2 D(\lambda), \tag{A 36}$$

where
$$g(\lambda) = -F_0\lambda^{\frac{1}{2}}[I_0(\mu_2 r)\{I_0(\mu_1 a)\,K_1(\mu_2 a) + (k_1/\kappa k_2)\,I_1(\mu_1 a)\,K_0(\mu_2 a)\} + K_0(\mu_2 r)\{I_0(\mu_1 a)\,I_1(\mu_2 a) - (k_1/\kappa k_2)\,I_1(\mu_1 a)\,I_0(\mu_2 a)\}]. \quad (A\ 37)$$

The residues at $\lambda = 0$ and $\lambda = -\kappa_1\alpha_s^2$ are, respectively,

$$\mathrm{Res}\,(e^{\lambda t}\bar{v}_2)_{\lambda=0} = [(d/d\lambda)\{e^{\lambda t}g(\lambda)/D(\lambda)\}]_{\lambda=0} = \frac{g(0)}{D(0)}\left\{t + \frac{g'(0)}{g(0)} - \frac{D'(0)}{D(0)}\right\}, \quad (A\ 38)$$

where
$$g(0) = -F_0(\kappa_2^{\frac{1}{2}}/a), \quad (A\ 39)$$

$$g'(0) = -F_0(\kappa_2^{\frac{1}{2}}/a)\left[\tfrac{1}{4}\frac{a^2}{\kappa_1} + \tfrac{1}{4}\frac{r^2-a^2}{\kappa_2} + \tfrac{1}{2}a^2\left\{\frac{k_1}{k_2}\frac{1}{\kappa_1} - \frac{1}{\kappa_2}\right\}\ln\frac{r}{a}\right] \quad (A\ 40)$$

and
$$\mathrm{Res}\,(e^{\lambda t}\bar{v}_2)_{\lambda=-\kappa_1\alpha_s^2} = [e^{\lambda t}g(\lambda)/(d/d\lambda)\{\lambda^2 D(\lambda)\}]_{\lambda=-\kappa_1\alpha_s^2} = e^{-\kappa_1\alpha_s^2 t}\,g(-\kappa_1\alpha_s^2)\,\Phi(\alpha_s), \quad (A\ 41)$$

where $\Phi(\alpha_s)$ has been defined in (A 31).

Since

$$g(-\kappa_1\alpha_s^2) = \tfrac{1}{2}F_0\,\pi\kappa_1^{\frac{1}{2}}\alpha_s[J_0(r\kappa\alpha_s)\{J_0(a\alpha_s)\,Y_1(a\kappa\alpha_s) - (k_1/\kappa k_2)\,J_1(a\alpha_s)\,Y_0(a\kappa\alpha_s)\} - Y_0(r\kappa\alpha_s)\{J_0(a\alpha_s)\,J_1(a\kappa\alpha_s) - (k_1/\kappa k_2)\,J_1(a\alpha_s)\,J_0(a\kappa\alpha_s)\}], \quad (A\ 42)$$

equation (A 41) becomes

$$\mathrm{Res}\,(e^{\lambda t}\bar{v}_2)_{\lambda=-\kappa_1\alpha_s^2} = 2bF_0\,e^{-\kappa_1\alpha_s^2 t}\,(\tfrac{1}{2}\pi\kappa a\alpha_s)\,g_1(\alpha_s)\,\Psi(\alpha_s), \quad (A\ 43)$$

with $\Psi(\alpha_s)$ defined in (A 33) and

$$g_1(\alpha_s) = g(-\kappa_1\alpha_s^2)/(\tfrac{1}{2}F_0\,\pi\kappa_1^{\frac{1}{2}}\alpha_s). \quad (A\ 44)$$

We obtain from (A 38) and (A 43),

$$v_2 = \mathrm{Res}\,(e^{\lambda t}\bar{v}_2)_{\lambda=0} + \sum_{s=1}^{\infty}\mathrm{Res}\,(e^{\lambda t}\bar{v}_2)_{\lambda=-\kappa_1\alpha_s^2}, \quad (A\ 45)$$

of which an explicit expression is given in (9).

The solutions of the thermal conduction equations for a composite slab (appendix B) and a composite sphere (appendix C) are similar to that given above. A brief note will be appropriate with regard to the derivation of these solutions. By transforming the variables $v_1$ and $v_2$ in appendix C to a new set of variables $u_1$ and $u_2$ with the relations $u_1 = rv_1$ and $u_2 = rv_2$, the equations (C 1 and C 2) become new equations for $u_1$ and $u_2$ that have the same form as (B 1) and (B 2) appearing in appendix B. The fundamental set of solutions of the subsidiary equations derived from (B 1) and (B 2) are hyperbolic sine and cosine functions instead of the modified Bessel functions that are the basic solutions of (A 2) and (A 3). Also, as a result of the variable transformations, the subsidiary initial and boundary conditions corresponding to (C 3) through (C 7) assume a slightly more complicated form than those derived from (B 3) through (B 7). Except for these differences, the solution's derivation is analogous to that outlined in appendix A, and the results as indicated in appendixes B and C are reached without difficulty.

## Appendix B. Conduction of heat in the composite slab of one material for $|x| \leqslant a$ and of another for $a \leqslant |x| \leqslant b$; zero initial temperature; constant heat flux $\mp F_0$ at $x = \pm b$ for time $t > 0$

Let $v_1$, $k_1$, $\rho_1$, $c_1$ and $\kappa_1 = k_1/\rho_1 c_1$ be the temperature, thermal conductivity, density, specific heat and thermal diffusivity in the inner slab $|x| \leqslant a$ and $v_2$, $k_2$, $\rho_2$, $c_2$ and $\kappa_2 = k_2/\rho_2 c_2$ the corresponding quantities in the outer slab $a \leqslant |x| \leqslant b$ (figure B 1). Since the problem is symmetric with respect to $x = 0$, without loss of generality we can restrict the region under discussion to $0 \leqslant x \leqslant b$. The solution in the region $-b \leqslant x \leqslant 0$ will be obtained by changing the sign of $-F_0$, $a$, $b$ and $x$ in the solution for $0 \leqslant x \leqslant b$.

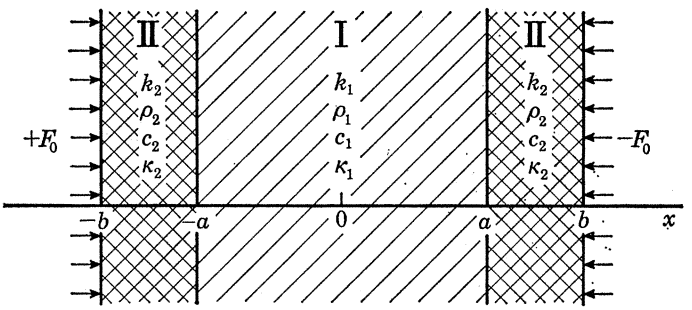


Figure B 1. Thermal conduction in a composite slab. Inner slab: thickness, $2a$; thermal conductivity, $k_1$; density, $\rho_1$; specific heat, $c_1$; thermal diffusivity, $\kappa_1$. Outer slabs: thickness, $b - a$; thermal conductivity, $k_2$; density, $\rho_2$; specific heat, $c_2$; thermal diffusivity, $\kappa_2$. Initial temperature zero. A constant heat flux $\mp F_0$ at the outer boundaries $x = \pm b$ for time $t > 0$.

The equations to be solved are

$$\frac{\partial^2 v_1}{\partial x^2} - \frac{1}{\kappa_1}\frac{\partial v_1}{\partial t} = 0, \quad 0 \leqslant x \leqslant a, \quad t > 0, \tag{B 1}$$

$$\frac{\partial^2 v_2}{\partial x^2} - \frac{1}{\kappa_2}\frac{\partial v_2}{\partial t} = 0, \quad a \leqslant x \leqslant b, \quad t > 0, \tag{B 2}$$

with the conditions

$$k_2 \partial v_2/\partial x = -F_0, \quad x = b, \quad t > 0, \tag{B 3}$$

$$v_1 = v_2, \quad x = a, \quad t > 0, \tag{B 4}$$

$$k_1 \partial v_1/\partial x = k_2 \partial v_2/\partial x, \quad x = a, \quad t > 0, \tag{B 5}$$

$$\partial v_1/\partial x = 0, \quad x = 0, \quad t > 0, \tag{B 6}$$

and

$$v_1 = 0\,(0 \leqslant x \leqslant a), \quad v_2 = 0(a \leqslant x \leqslant b), \quad t = 0. \tag{B 7}$$

The solutions are:

$$v_1 = -F_0 \left[ \frac{t + x^2/2\kappa_1}{\frac{k_1}{\kappa_1}a + \frac{k_2}{\kappa_2}(b-a)} - \frac{\frac{k_1}{\kappa_1}\left\{\frac{a^3}{6\kappa_1} + \frac{a(b-a)^2}{2\kappa_2}\right\} + \frac{k_2}{\kappa_2}\left\{\frac{a^2(b-a)}{2\kappa_1} + \frac{(b-a)^3}{6\kappa_2}\right\}}{\left\{\frac{k_1}{\kappa_1}a + \frac{k_2}{\kappa_2}(b-a)\right\}^2} - \sum_{s=1}^{\infty} \mathrm{e}^{-\kappa_1 \alpha_s^2 t} \cos x\alpha_s \, \Psi(\alpha_s) \right], \tag{B 8}$$

$$v_2 = -F_0\left[\frac{t+\frac{a^2}{2\kappa_1}+\frac{k_1}{k_2}\frac{a(x-a)}{\kappa_1}+\frac{(a-x)^2}{2\kappa_2}}{\frac{k_1}{\kappa_1}a+\frac{k_2}{\kappa_2}(b-a)} - \frac{\frac{k_1}{\kappa_1}\left\{\frac{a^3}{6\kappa_1}+\frac{a(b-a)^2}{2\kappa_2}\right\}+\frac{k_2}{\kappa_2}\left\{\frac{a^2(b-a)}{2\kappa_1}+\frac{(b-a)^3}{6\kappa_2}\right\}}{\left\{\frac{k_1}{\kappa_1}a+\frac{k_2}{\kappa_2}(b-a)\right\}^2}\right.$$

$$\left. -\sum_{s=1}^{\infty} e^{-k_1\alpha_s^2 t}\{\cos a\alpha_s \cos(x-a)\kappa\alpha_s - (k_1/\kappa k_2)\sin a\alpha_s \sin(x-a)\kappa\alpha_s\}\,\Psi(\alpha_s)\right], \tag{B 9}$$

where $\kappa \equiv \sqrt{(\kappa_1/\kappa_2)}$,

$$\Psi(\alpha_s)^{-1} \equiv \tfrac{1}{2}\kappa_1\alpha_s^2\left[\left\{\frac{k_1}{\kappa_1}a+\frac{k_2}{\kappa_2}(b-a)\right\}\cos a\alpha_s \cos(b-a)\kappa\alpha_s - \left\{\frac{k_1}{\kappa_1}\kappa(b-a)+\frac{k_2}{\kappa\kappa_2}a\right\}\sin a\alpha_s \sin(b-a)\kappa\alpha_s\right], \tag{B 10}$$

and $\alpha_s$, $s = 1, 2, \ldots$ are the positive roots of

$$\cos a\alpha \sin(b-a)\kappa\alpha + (k_1/\kappa k_2)\sin a\alpha \cos(b-a)\kappa\alpha = 0 \tag{B 11}$$

for $\alpha$, including the common roots, if any, of

$$\sin a\alpha = \sin(b-a)\kappa\alpha = 0 \tag{B 12}$$

and

$$\cos a\alpha = \cos(b-a)\kappa\alpha = 0 \tag{B 13}$$

for $\alpha$.

The equations (B 12) have common roots if and only if $(b-a)\kappa/a$ is rational. Suppose $(b-a)\kappa/a = m/n$, where $m$ and $n$ are positive integers mutually irreducible. Then the common roots of (B 12) are $\alpha_s' = s'\pi M$, $s' = 1, 2, \ldots$ where $M = n/a = m/(b-a)\kappa$. In the case of both $m$ and $n$ being odd integers, equation (B 13) also has common roots: $\alpha_s'' = \frac{1}{2}s''\pi M$, $s'' = 1, 2, \ldots$. The summations with respect to $s$ in (B 8) and (B 9) must include the terms corresponding to these roots when they exist.

## Appendix C. Conduction of heat in the composite sphere of one material for $0 \leqslant r \leqslant a$ and of another for $a \leqslant r \leqslant b$; zero initial temperature, constant heat flux $-F_0$ at $r = b$ for time $t > 0$

Let $v_1$, $k_1$, $\rho_1$, $c_1$ and $\kappa_1 = k_1/\rho_1 c_1$ be the temperature, thermal conductivity, density, specific heat and thermal diffusivity for the inner sphere $0 \leqslant r \leqslant a$ and $v_2, k_2, \rho_2, c_2$ and $\kappa_2 = k_2/\rho_2 c_2$ the corresponding quantities for the outer sphere $a \leqslant r \leqslant b$.

The equations to be solved are

$$\frac{\partial^2 v_1}{\partial r^2}+\frac{2}{r}\frac{\partial v_1}{\partial r}-\frac{1}{\kappa_1}\frac{\partial v_1}{\partial t} = 0, \quad 0 \leqslant r \leqslant a, \quad t > 0, \tag{C 1}$$

$$\frac{\partial^2 v_2}{\partial r^2}+\frac{2}{r}\frac{\partial v_2}{\partial r}-\frac{1}{\kappa_2}\frac{\partial v_2}{\partial t} = 0, \quad a \leqslant r \leqslant b, \quad t > 0, \tag{C 2}$$

with the conditions

$$k_2\,\partial v_2/\partial r = -F_0, \quad r = b, \quad t > 0, \tag{C 3}$$

$$v_1 = v_2, \quad r = a, \quad t > 0, \tag{C 4}$$

$$k_1\,\partial v_1/\partial r = k_2\,\partial v_2/\partial r, \quad r = a, \quad t > 0, \tag{C 5}$$

$$\partial v_1/\partial r = 0, \quad r = 0, \quad t > 0, \tag{C 6}$$

and
$$v_1 = 0\,(0 \leqslant r \leqslant a), \quad v_2 = 0\,(a \leqslant r \leqslant b), \quad t = 0. \tag{C 7}$$

The solutions are

$$v_1 = -3b^2F_0\left[\frac{t+\dfrac{r^2}{6\kappa_1}}{\dfrac{k_1}{\kappa_1}a^3+\dfrac{k_2}{\kappa_2}(b^3-a^3)}\right.$$
$$-\frac{\dfrac{k_1}{\kappa_1}\left\{\dfrac{a^5}{10\kappa_1}+\dfrac{a^2(b-a)^2(2b+a)}{6\kappa_2}\right\}+\dfrac{k_2}{\kappa_2}\left\{\dfrac{a^2(b-a)^3+3a^3b(b-a)}{6\kappa_1}+\dfrac{5ab(b-a)^3+(b-a)^5}{10\kappa_2}\right\}}{\left\{\dfrac{k_1}{\kappa_1}a^3+\dfrac{k_2}{\kappa_2}(b^3-a^3)\right\}^2}$$
$$\left.-\frac{1}{r}\sum_{s=1}^{\infty}\mathrm{e}^{-\kappa_1\alpha_s^2t}\sin r\alpha_s\,\Psi(\alpha_s)\right], \tag{C 8}$$

$$v_2 = -3b^2F_0\left[\frac{t+\dfrac{a}{r}\left\{\dfrac{a^2}{6\kappa_1}+\left(1+2\dfrac{k_1}{k_2}\right)\dfrac{a(r-a)}{6\kappa_1}+\dfrac{(r-a)^2(2+r/a)}{6\kappa_2}\right\}}{\dfrac{k_1}{\kappa_1}a^3+\dfrac{k_2}{\kappa_2}(b^3-a^3)}\right.$$
$$-\frac{\dfrac{k_1}{\kappa_1}\left\{\dfrac{a^5}{10\kappa_1}+\dfrac{a^2(b-a)^2(2b+a)}{6\kappa_2}\right\}+\dfrac{k_2}{\kappa_2}\left\{\dfrac{a^2(b-a)^3+3a^3b(b-a)}{6\kappa_1}+\dfrac{5ab(b-a)^3+(b-a)^5}{10\kappa_2}\right\}}{\left\{\dfrac{k_1}{\kappa_1}a^3+\dfrac{k_2}{\kappa_2}(b^3-a^3)\right\}^2}$$
$$-\frac{1}{r}\sum_{s=1}^{\infty}\mathrm{e}^{-\kappa_1\alpha_s^2t}\left\{\sin a\alpha_s\cos(r-a)\,\kappa\alpha_s\right.$$
$$\left.\left.+\frac{1}{\kappa}\left(\frac{k_1}{k_2}\cos a\alpha_s+\frac{k_2-k_1}{k_2}\frac{\sin a\alpha_s}{a\alpha_s}\right)\sin(r-a)\,\kappa\alpha_s\right\}\Psi(\alpha_s)\right], \tag{C 9}$$

where $\kappa \equiv (\kappa_1/\kappa_2)^{\frac{1}{2}}$ as before,

$$\Psi(\alpha_s)^{-1} \equiv \tfrac{3}{2}\kappa_1\alpha_s^2\left[\frac{1}{\kappa}\left\{\frac{k_2-k_1}{\kappa_1\alpha_s^2}+\frac{k_1}{\kappa_2}b(b-a)+\frac{k_2}{\kappa_2}ab\right\}\cos a\alpha_s\sin(b-a)\,\kappa\alpha_s\right.$$
$$+\left\{\frac{k_2-k_1}{\kappa_1\alpha_s^2}\frac{b-a}{a}+\frac{k_1}{\kappa_1}ab+\frac{k_2}{\kappa_2}b(b-a)\right\}\sin a\alpha_s\cos(b-a)\,\kappa\alpha_s$$
$$-\frac{1}{\alpha_s}\left\{\frac{k_2-k_1}{\kappa_1}(b-a)\right\}\cos a\alpha_s\cos(b-a)\,\kappa\alpha_s$$
$$\left.-\frac{1}{\kappa\alpha_s}\left\{\frac{k_1}{\kappa_1}a+\frac{k_2-k_1}{\kappa_1a\alpha_s^2}-\frac{k_2-k_1}{\kappa_2}\frac{b(b-a)}{a}+\frac{k_2}{\kappa_2}a\right\}\sin a\alpha_s\sin(b-a)\,\kappa\alpha_s\right], \tag{C 10}$$

and $\alpha_s$, $s = 1, 2, \ldots$ are the positive roots of

$$\sin(b-a)\,\kappa\alpha[a\alpha\cos a\alpha-\{1-(k_2/k_1)\,(1+ab\kappa^2\alpha^2)\}\sin a\alpha]$$
$$= b\kappa\alpha\cos(b-a)\,\kappa\alpha\,[a\alpha\cos a\alpha-\{1-(k_2/k_1)\,(b-a)/b\}\sin a\alpha] \tag{C 11}$$

for $\alpha$.

The research was conducted in close cooperation with N.A.S.A.'s Lunar Sample Analysis Planning Team. According to their recommendations, a number of improvements were incorporated in our experimental arrangements and procedures. The members of the team who contributed most to the project include Dr P. Bell, Dr B. Doe, Dr J. Adams, Dr N. Toksöz, Dr. B. Burnett, Dr P. Eberhardt, Dr C. Simonds, Dr S. Haggerty, Dr S. Solomon, Dr E. Schreiber, Dr G. Reed, Dr S. Chang, Dr D. Papanastassiou, Dr R. Housley, Dr K. Marti, and Dr D. Heymann. The experimental work was conducted at N.A.S.A.'s L. B. Johnson Space Center with the Lunar Sample Curator's facility, by courtesy of the Center's Earth and Planetary Science Division chiefs, the late Professor P. Gast and Dr L. Haskin and the Lunar Sample Curator, Dr M. Duke. Technical support was provided by a Johnson Space Center contractor Lockheed Electronic Corporation's Planetary and Earth Sciences Department under the direction of Mr N. Allen and Mr F. Gibbons. Johnson Space Center's engineers and technicians are acknowledged for the following assistance: Mr T. Grubbs and Mr C. Allton of the Engineering Division for designing the prototype experimental arrangement, Mr R. Bullock of the Structure and Mechanics Division for measuring the thermal emissivity by infrared reflectometer, and Mr R. Stubblefield of the Engineering Standards and Calibrations Laboratory for calibrating the thermocouples used in the study. All information concerning the thermophysical properties of the titanium alloy Ti–6Al–4V was provided by Dr R. Powell and Dr J. Hust of the Institute for Basic Standards of the National Bureau of Standards. Information and suggestions given by Dr A. Wechsler, Dr J. Lindsay and Dr D. Colvin were most helpful in the earliest stage of the project. We are grateful for the personal encouragement given by Dr D. Strangway, Dr D. Carrier, Dr G. Heiken and Dr W. Mendell. Financial support was provided by the National Aeronautics and Space Administration under grants NGR 33-008-169, NGR 33-008-174 and NGR 33-008-177.

## References

Carrier, W. D. III, Mitchell, J. K. & Mahmood, A. 1973 *J. Soil Mech. Fdns Div. Am. Soc. civ. Engrs* **99**, 813–832.
Carslaw, H. S. & Jaeger, J. C. 1959 *Conduction of heat in solids* (2nd ed.), 510 pp. Oxford: Clarendon Press.
Cremers, C. J. 1972 *Proc. Lunar Sci. Conf.* 3*rd*, pp. 2611–2617.
Cremers, C. J. 1975 *J. geophys. Res.* **80**, 4466–4470.
Cremers, C. J. & Birkebak, R. C. 1971 *Proc. Lunar Sci. Conf.* 2*nd*, pp. 2311–2315.
Cremers, C. J. & Hsia, H. S. 1973 *Proc. Lunar Sci. Conf.* 4*th*, pp. 2359–2464.
Cremers, C. J. & Hsia, H. S. 1974 *Proc. Lunar Sci. Conf.* 5*th*, pp. 2703–2708.
Cremers, C. J., Birkebak, R. C. & Dawson, J. P. 1970 *Proc. Apollo* 11, *Lunar Sci. Conf.*, pp. 2045–2050.
Fountain, J. A. & West, E. A. 1975 In *Lunar Science*, vol. VI, pp. 268–270. Lunar Science Institute, Houston, Texas.
Gold, T., O'Leary, B. T. & Campbell, M. 1971 *Proc. Lunar Sci. Conf.* 2*nd*, pp. 2173–2181.
Görz, H., White, E. W., Johnson, G. G. Jr. & Pearson, M. W. 1972 *Proc. Lunar Sci. Conf.* 3*rd*., pp. 3195–3200.
Gröber, H., Erk, S. & Gribull, V. 1961 *Fundamentals of Heat Transfer*, 527 pp. New York: McGraw-Hill.
Hemingway, B. S., Robie, R. A. & Wilson, W. H. 1973 *Proc. Lunar Sci. Conf.* 4*th*, pp. 2481–2487.
Jaeger, J. C. 1941 *Phil. Mag.* **32**, 324–335.
King, A. E. Jr., Butler, J. C. & Carman, M. F. Jr. 1972 *Proc. Lunar Sci. Conf.* 3*rd*, pp. 673–686.
Langseth, M. G., Keihm, S. J. & Peters, K. 1976 *Proc. Lunar Sci. Conf.* 7*th*, pp. 3143–3171.
Mitchell, J. K., Bromwell, L. G., Carrier III, W. D., Costes, N. C. & Scott, R. F. 1972 *J. geophys. Res.* **77**, 5641–5664.
Mitchell, J. K., Carrier, W. D. III, Costes, N. C., Houston, W. N., Scott, R. F. & Hovland, H. J. 1973 In *Apollo* 17 *Preliminary Science Report*, ch. 8, pp. 1–22. National Aeronautics and Space Administration, Washington D.C.
Robie, R. A. & Hemingway, B. S. 1971 *Proc. Lunar Sci. Conf.* 2*nd*, pp. 2361–2365.
Robie, R. A., Hemingway, B. S. & Wilson, W. H. 1970 *Proc. Apollo* 11 *Lunar Sci. Conf.*, pp. 2361–2367.
Scott, R. F., Carrier W. D. III, Costes, N. C. & Mitchell, J. K. 1971 *Geotechnique* **21**, 1–14.
Scott, R. W., Fountain, J. A. & West, E. A. 1973 *Rev. scient. Instrum.* **44**, 1058–1063.
Watson, G. N. 1966 *A treatise on the theory of Bessel functions*, 804 pp., New York: Cambridge University Press.
Wechsler, A. E. & Glaser, P. E. 1965 *Icarus* **4**, 335–352.


PHILOSOPHICAL TRANSACTIONS OF THE ROYAL SOCIETY A MATHEMATICAL, PHYSICAL & ENGINEERING SCIENCES